Model complexity and optimization trade-offs in the design and scheduling of hybrid hydrogen-battery systems

Energy Conversion and Management 344 (2025) 120306

Contents lists available at ScienceDirect

Energy Conversion and Management

journal homepage: www.elsevier.com/locate/enconman

Research Paper

Model complexity and optimization trade-offs in the design and scheduling of hybrid hydrogen-battery systems

Elena Rozzi [a,b,*], Alberto Grimaldi [a,b], Francesco D. Minuto [a,b], Andrea Lanzini [a,b]

[a] Department of Energy, Politecnico di Torino, Corso Duca degli Abruzzi 24, 10129 Torino, Italy
[b] Energy Center Lab, Politecnico di Torino, Via Paolo Borsellino 38/16, 10138 Torino, Italy

ARTICLE INFO

Keywords:
MILP optimization
Rolling horizon
Particle Swarm Optimization
Power-to-hydrogen
Piecewise Affine linearization
Battery Degradation

ABSTRACT

The production of hydrogen from renewable sources could play a significant role in supporting the transition toward a decarbonized energy system. This study has involved investigating optimization strategies – mixed-integer linear programming (MILP), a hybrid particle swarm optimization (PSO)-MILP framework, and PSO combined with a rule-based energy management strategy (EMS) – applied to a power-to-hydrogen system for industrial applications. The analysis evaluates the levelized cost of hydrogen production (LCOH), carbon emissions, and the impact of key factors, such as battery degradation, electrolyzer efficiency, real-time pricing, and hydrogen load management. The obtained results indicated that the MILP-based models achieved moderate LCOH values (10.1–10.7 €/kg) but incurred higher CO_2 emissions (20.2–24.6 kt/y). Instead, the PSO model, combined with the rule-based EMS, lowered emissions to 14.3 kt/y (a 27–45% reduction), albeit with a higher LCOH (11.6 €/kg). The hybrid PSO-MILP models struck a balance, achieving LCOH values of between 9.2 and 9.7 €/kg, with CO_2 emissions of 19.7–20.3 kt/y, as they benefited from the integration of piecewise affine linearization for modeling electrolyzer efficiency and battery degradation. In terms of computational efforts, the MILP-based models required more than 48 h to converge, while the PSO-MILP models completed within 27–35 h, and the PSO model with rule-based EMS achieved results in 1.5 h. These findings offer guidance that can be used to select the most suitable optimization method on the basis of the desired performance targets, resource constraints, and computational complexity, thereby contributing to the design of more sustainable energy systems.

1. Introduction

Hydrogen energy is increasingly gaining attention as a clean, versatile, and storable energy solution, especially for the decarbonization of sectors in which emissions are hard to abate, such as heavy industries and high-temperature industrial processes [1]. In 2022, the industry sector directly emitted 9 Gt of CO_2, thereby accounting for 25 % of the global energy-related CO_2 emissions [2]. Hydrogen is widely used as a feedstock and reducing agent in refineries, for chemical production, and in steel industries. However, other potential applications – including the production of hydrogen-based fuels (e.g., ammonia, synthetic hydrocarbons), the upgrading of biofuels, the provision of high-temperature heat for industrial processes, hydrogen-based direct reduced iron and electricity storage and generations – have yet to be adopted at an industrial scale. This is due to their current lack of competitiveness with fossil fuels and to the lack of maturity of the required technologies, but these applications are expected to grow to comply with the decarbonization efforts [3]. In 2022, the global production of hydrogen reached 95 Mt, but less than 1 Mt (0.7 % of the global production) was derived from low-emission processes that involved carbon capture, and less than 100 kt of hydrogen was produced through water electrolysis [3,4]. Nevertheless, the electrolyzer installed capacity grew by more than 20 % [5], and the demand for low-emissions hydrogen is expected to reach 70 Mt by 2030 [4].

Therefore, in order to meet the rising demand for green hydrogen and to effectively scale up production, it is essential to manage the hydrogen production process in alignment with the demand. The inherent variability and intermittency of such renewable energy sources (RES) as wind and solar make it necessary to adopt an integrated approach that includes energy storage solutions – such as batteries, hydrogen or hybrid systems – to ensure a consistent hydrogen supply from power-to-hydrogen (P2H) systems [6].

Battery energy storage systems (BESS) are primarily used for short-term energy storage, due to their relatively low storage capacity, low energy density (30 Wh/kg), limited lifespan, and their tendency to self-

* Corresponding author at: Department of Energy, Politecnico di Torino, Corso Duca degli Abruzzi 24, 10129 Torino, Italy.
E-mail address: elena.rozzi@polito.it (E. Rozzi).

https://doi.org/10.1016/j.enconman.2025.120306
Received 25 February 2025; Received in revised form 25 July 2025; Accepted 29 July 2025
Available online 15 August 2025

Nomenclature

Abbreviations

ABC	Artificial Bee Colony
ACO	Ant Colony Optimization
ALO	Ant Lion Optimizer
ARERA	Autorità di Regolazione per Energia Reti e Ambiente (Regulatory Authority for Energy Networks and the Environment)
AVOA	African Vulture Optimization Algorithm
BB-BC	Big Bang-Big Crunch
BBO	Biogeography-Based Optimization
BESS	Battery Energy Storage System
CAPEX	Capital Expenditure
CGH_2	Compressed Hydrogen Storage
CRF	Capital Recovery Factor
CS	Cuckoo Search
DA	Dragonfly Algorithm
DC	Direct Current
DOD	Depth of Discharge
EL	Electrolyzer
EMS	Energy Management Strategy
GA	Genetic Algorithm
GAMS	General Algebraic Modeling System
GME	Gestore dei Mercati Energetici (Manager of the Energy Market)
GOA	Grasshopper Optimization Algorithm
GWO	Grey Wolf Optimizer
HS	Harmony Search,
IC	Imperialist Competitive
IWO	Invasive Weed Optimization
KKT	Karush-Kuhn-Tucker
KPI	key performance indicators
LCOH	Levelized Cost of Hydrogen
LP	Linear Programming
MFO	Moth-flame Optimization
MILP	Mixed-Integer Linear Programming
MINLP	Mixed-Integer Non-Linear Programming
MISOCP	Mixed Integer Second Order Conic Programming
MVO	Multi-Verse Optimizer
NREL	National Renewable Energy Laboratory
O&M	Operational and Maintenance
OPEX	Operational Expenditure
P2H	Power-to-Hydrogen
PEM	Proton Exchange Membrane
PLC	Programmable Logic Controller
PSO	Particle Swarm Optimization
PV	Photovoltaic
PVGIS	Photovoltaic Geographical Information System
PWA	Piecewise affine
QP	Quadratic Programming
RB	Rule-based
RCA	Rainflow Counting Algorithm
RES	Renewable Energy Source
RMSE	Root Mean Squared Error
SC	Supercapacitor
SCE	Shuffled Complex Evolution
SOC	State of Charge
SSA	Salp Swarm Algorithm
TLBO	Teaching–Learning Based Optimization

Parameters economic and financial parameters

C_{inv}	Capital investment [€/kW] or [€/kWh]
C_{inv}^{ann}	Annualized capital costs [€/kW] or [€/kWh]
$C_{O\&M}$	Operation and maintenance costs [€/kW] or [€/kWh]
C_{rep}	Replacement costs [€/kW] or [€/kWh]
C_{rep}^{ann}	Annualized replacement costs [€/kW] or [€/kWh]
R	Revenues [€]
CRF	Capital recovery factor [-]
SFF	Sinking fund factor [-]
F_{rep}	Number of replacements [-]
r	Interest rate [%]
n	Project lifetime [years]
y	Technology lifetime [years]
I_{CO_2}	Average emission intensity [g_{CO2}/kWh]
f_{obj}	Objective function [-]
w_a, w_b	Weighting factors [-]

Energy storage parameters

$E_{BESS,nom}$	Nominal BESS energy capacity [kWh]
$E_{BESS,rem}$	Hourly remaining capacity of BESS [kWh]
$E_{BESS,stored}$	Hourly energy stored in the BESS [kW]
$E_{CGH_2,nom}$	Nominal CGH_2 energy capacity [kWh]
$E_{CGH_2,stored}$	Hourly energy stored in the CGH_2 [kWh]
$P_{BESS,ch}$	Hourly charging power of the BESS [kW]
$P_{BESS,dc}$	Hourly discharging power of the BESS [kW]
$P_{CGH_2,ch}$	Hourly charging power of the CGH_2 [kW]
$P_{CGH_2,dc}$	Hourly discharging power of the CGH_2 [kW]
$P_{BESS,nom}$	Nominal BESS power capacity [kW]
$P_{EL,aux}$	Hourly auxiliary power for the electrolyzer [kW]
$P_{EL,in}$	Hourly electrolyzer power input [kW]
$P_{EL,out}$	Hourly electrolyzer power output [kW]
$P_{Grid,buy}$	Hourly power withdrawn from the grid [kW]
$P_{Grid,sell}$	Hourly power injected into the grid [kW]
$P_{H2,load}$	Hourly hydrogen demand [kW]
P_{PV}	Hourly photovoltaic power generation [kW]
$P_{PV,nom}$	Nominal PV power capacity [kW]
$P_{EL,nom}$	Nominal power capacity of the electrolyzer [kW]
$P_{H2,buy}$	Hourly hydrogen purchase [kW]
$SOC_{BESS,rem}$	Hourly remaining BESS state of charge [%]
cyc	Number of cycles performed by BESS [-]
η_{EL}	Electrolyzer efficiency [%]
LHV_{H2}	Lower heating value of hydrogen [kWh/kg]
n_{H2}	Number of moles of hydrogen [mol]

Optimization and KPIs

H	Optimization horizon [hours]
U	Update interval [hours]
$PV_{surplus}$	PV surplus index [%]
$ImportIndex$	Electricity purchase index [%]
$BESSutilization$	Ratio of energy delivered by BESS [%]
$CGH_2utilization$	Ratio of energy delivered by CGH_2 [%]
$SOC_{BESS,ave}$	Average state of charge of BESS [%]
$SOF_{CGH_2,ave}$	Average state of charge of CGH_2 [%]
$\eta_{EL,ave}$	Average efficiency of the electrolyzer [%]
R^2	coefficient of determination
Δt	Timestep [hours]

PSO algorithm parameters

w	Inertia weight in the PSO algorithm [-]
c_1	Cognitive acceleration coefficient (self-influence) [-]
c_2	Social acceleration coefficient (swarm influence) [-]
x_{ij}	Position of particle i in dimension j [-]
v_{ij}	Velocity of particle i in dimension j [-]
y_{ij}	Best-known position of particle i in dimension j [-]
$\hat{y}_j$	Global best position in dimension j [-]
$r_{1j}, r_{2,j}$	Random numbers for cognitive and social components [-]

discharge when not connected to a load. On the other hand, compressed hydrogen storage (CGH_2) is particularly suitable for long-term and seasonal storage, as it offers a high storage capacity, scalability, and a significantly higher gravimetric energy density, together with a lower heating value of 33.33 kWh/kg [7].

The economic viability and environmental sustainability for green hydrogen hinges on robust optimization models that are capable of coordinating production and storage, maximizing renewable energy utilization, and minimizing costs. However, despite some noteworthy advances in optimization approaches, several key challenges remain. The variability of renewable energy, the modeling of battery degradation, and the non-linear representation of electrolyzer efficiency considered together pose high computational complexity. Additionally, conflicting objectives – such as minimizing production costs, reducing carbon emissions, ensuring operational feasibility, and containing computational requirements – lack standardized balancing criteria. Thus, it is still unclear whether linear programming, metaheuristics or hybrid methods represent the most effective strategy for large-scale P2H systems.

A broad spectrum of optimization approaches have been extensively explored in recent years, notably mixed-integer linear programming (MILP) and metaheuristic algorithms such as particle swarm optimization (PSO), genetic algorithms (GA), ant colony optimization (ACO), moth-flame optimization (MFO), and grey wolf optimizer (GWO). MILP is commonly employed for operational scheduling task due to its ability to efficiently handle linear constraints and discrete decision variables, ensuring optimal or near-optimal solutions within acceptable computational timeframes [8–16]. For instance, Diabate et al. [17] developed a MILP approach explicitly incorporating battery degradation, demonstrating its potential to effectively manage daily operational costs by prolonging battery lifespan. Similarly, Giovanniello and Wu [18] proposed a two-step MILP framework highlighting the economic advantage of hybrid battery-hydrogen storage systems, emphasizing significant enhancements in system reliability and cost-efficiency. Further contributions, such as those by Deng et al. [19], Shi et al. [20], and Hassan et al. [21], extended MILP methodologies to multi-energy microgrids, reinforcing their effectiveness in simultaneously addressing cost and emission objectives.

Conversely, metaheuristic algorithms have primarily excelled in system sizing and design optimization, given their inherent flexibility and robustness in navigating complex, multi-dimensional, and non-linear solution spaces. Eriksson and Gray [22] presented a thorough overview of hybrid renewable energy systems optimized through metaheuristic functions, highlighting their ability to manage the intricate trade-offs among technical, economic, and environmental criteria. Similarly, Phan-Van et al. [23] extensively compared eight distinct metaheuristic optimization algorithms for hydrogen-battery integrated systems, revealing the superiority of PSO in terms of convergence rate and optimal solution quality. Furthermore, Mohseni et al. [24] validated the rapid convergence and solution reliability of PSO and MFO when applied to standalone hydrogen-based microgrids, confirming their applicability for complex, multi-objective design scenarios. Studies by Amoussou et al. [25] and HassanzadehFard et al. [26] further supported these findings, demonstrating the capability of metaheuristics to efficiently handle diverse and challenging system configurations, ranging from integrated PV-wind-hydrogen storage to waste-to-hydrogen applications.

Recognizing the complementary strengths of MILP and metaheuristics, recent research has shifted towards hybrid methodologies to leverage on the strengths of both methods to handle nonlinearity and complexity more effectively. Such hybrid approaches strategically deploy MILP for operational scheduling, exploiting its efficiency in time-dependent optimizations, while metaheuristics are utilized primarily for optimal system sizing and initial solution identification, significantly enhancing computational performance and accuracy. Kim et al. [27] demonstrated that initializing PSO algorithms with solutions generated by MILP markedly improved microgrid scheduling outcomes compared to either method used independently. Similarly, Han et al. [28], developed a hybrid PSO-MILP co-optimization framework tailored explicitly to microgrids featuring combined battery-hydrogen storage. Their finding confirmed substantial reductions in system costs and emissions compared to single-method frameworks. Additionally, Micangeli et al. [29] extensively compared single-layer MILP and hybrid PSO-MILP approaches, incorporating a rolling horizon strategy, highlighting marked improvements in computational time and solution precision by sequentially refining scheduling decisions.

Parallel to methodological innovations, dynamic optimization techniques, especially rolling horizon approaches, have been increasingly applied to renewable-based energy systems to effectively manage uncertainties and intermittency in renewable energy availability and load demands. This technique decomposes complex scheduling problems into sequentially solvable smaller sub-problems, enabling ongoing re-optimization as updated data becomes available. Rullo et al. [34] effectively employed a rolling horizon strategy in an off-grid hybrid renewable system, significantly reducing storage requirements and operational costs. Malysz et al. [35] also leveraged rolling horizon-based MILP approaches to optimize battery storage operation, successfully achieving simultaneous economic benefits, peak shaving, and improved battery lifespan. Further advancements by Elkazaz et al. [36] and Erichsen et al. [30] confirmed the efficacy of rolling horizon methodologies in enhancing renewable self-consumption, grid dependency management, and long-term storage preservation.

An additional layer of complexity arises from accurately representing critical nonlinear behaviors inherent in energy storage and conversion components, notably electrolyzer efficiency and battery degradation. To address these non-linearities within MILP frameworks, piecewise affine (PWA) linearizations have emerged as essential modeling techniques, allowing more precise operational scheduling and economic optimization [37–40]. Marocco et al. [41] applied PWA linearizations specifically to electrolyzer and fuel-cell efficiency curves, enhancing scheduling performance and resource utilization. Similarly, Neisen et al. [42] demonstrated that integrating PWA linearizations for electrolyzer efficiency significantly altered operational strategies, shifting operations towards more optimal efficiency ranges and positively impacting overall system economics. Gabrielli et al. [43] expanded on these methods by systematically validating PWA approximations against detailed non-linear models, highlighting their robustness in accurately capturing complex system dynamics, including temperature-dependent behavior and operational flexibility. Additionally, Keske et al. [44] and, Peñaranda et al. [45] successfully extended PWA modeling techniques specifically for battery degradation curves, demonstrating their efficacy in achieving accurate lifecycle assessments and economic optimization in energy arbitrage contexts.

Although previous studies have substantially advanced the state-of-art, several critical gaps remain. Specifically, a systematic and comprehensive comparative evaluation of alternative optimization strategies under realistic operating conditions, involving dynamic electricity pricing, highly variable hydrogen demand patterns, and fluctuating renewable generation profiles, has not been thoroughly addressed. Such a comparison is essential to identify the most effective trade-offs between economic objectives, emission reductions, operational feasibility, and computational complexity.

Table A1 highlights the types of storage systems analyzed, the optimization approaches adopted, the nonlinear modeling strategies employed, and their relevance to the current work. However, the simultaneous integration of rolling horizon strategies and PWA linearizations within hybrid optimization frameworks – particularly for systems combining battery and hydrogen storage and involving simultaneous optimization of component sizing and operational scheduling – has not yet been comprehensively explored. While previous studies on battery degradation modeling using MILP-based approaches typically assumed fixed battery sizes, optimizing battery design

introduces significant complexities. Specifically, when battery size becomes an optimization variable, the calculation of the state of charge (SOC) becomes inherently nonlinear, posing substantial challenges within MILP formulations traditionally adapted for linear problems.

This study explicitly addresses these critical methodological and practical gaps by rigorously comparing three distinct optimization configurations in a realistic, industrial-scale, grid-connected power-to-hydrogen (P2H) scenario:

1. MILP for integrated sizing and scheduling**:** this configuration ensures precise control, exploiting MILP's capability to efficiently handle linear constraints and discrete variables. Traditionally, MILP provides exact optimal or near-optimal solutions within acceptable computational times for linear models. However, when nonlinearities such as variable electrolyzer efficiency and battery degradation are introduced, MILP becomes computationally intensive and less scalable, as the solution deviates from true optimality due to necessary linear approximations.
2. Hybrid PSO-MILP (particle swarm optimization for sizing and MILP for operational scheduling)**:** in this hybrid configuration, PSO is used to explore the sizing decisions, while MILP optimizes the scheduling tasks. The choice of PSO, specifically, is strongly supported by extensive literature evidence, which highlights its superior performance over other metaheuristic optimization algorithms, such as GA, ACO, and MFO, in terms of both convergence speed and solution quality. Thus, PSO's effectiveness and robustness make it particularly suitable for efficiently navigating complex, nonlinear optimization landscapes, thereby enhancing the overall performance of hybrid optimization strategies. Furthermore, the rolling horizon approach is integrated to enable real-time decision-making and adaptivity to variable demand and renewable generation forecasts, extending its traditional battery-only applications to battery-hydrogen hybrid systems.
3. PSO with rule-based energy management strategy (EMS)**:** this method closely mirrors real-world engineering implementations where reduced computational burden and robustness in decision-making outweigh the pursuit of mathematical optimality. By relying on predefined operational rules and metaheuristic-based sizing, this configuration provides rapid, practical, and computationally less demanding solutions suitable for applications where near-optimal performance is acceptable.

This research intentionally escalates the complexity of the problem to better approximate real-world conditions, particularly by introducing critical nonlinearities such as electrolyzer efficiency curves and battery degradation dynamics. While it is known from previous literature that MILP algorithms are specifically adapted to linear problems and typically guarantee optimal solutions efficiently, their performance and computational demands increase significantly with the introduction of nonlinearities. Thus, the conventional view that MILP is always computationally less demanding than metaheuristics, needs reassessment under realistic operational complexities. In this regard, heuristic algorithms, although generally computationally intensive due to their reliance on population-based exploration methods, may provide solutions closer to real-world applicability by effectively handling highly nonlinear and complex system representations. In this context, hybrid optimization approaches, such as the combination of PSO and MILP, could effectively leverage the complementary strengths of both methodologies: the ability of metaheuristics to efficiently explore complex, nonlinear solution spaces, and the precision of MILP in solving linearized scheduling problems. Such hybrid approaches have the potential to achieve superior performance, balancing solution accuracy, computational efficiency, and practical feasibility under realistic and complex operating conditions.

Given these considerations, this study provides a detailed comparative assessment of MILP-based, metaheuristic-based, and hybrid optimization approaches applied to P2H systems, incorporating variable renewable energy inputs, real-time electricity pricing, and fluctuating hydrogen demand profiles. The investigation focuses on how different optimization strategies behave under increased problem complexity, highlighting the computational trade-offs and solution quality impacts introduced by nonlinear modelling choices.

The main methodological contributions and innovations of this study are explicitly articulated as follows:

- Systematic and comprehensive comparative analysis of MILP, hybrid MILP-PSO, and PSO-EMS optimization strategies under realistic industrial-scale operating conditions. This analysis explicitly evaluates the trade-offs between economic performance (levelized cost of hydrogen, LCOH), environmental objectives (carbon emission reductions), and computational complexity, providing clear guidelines on when a more complex and accurate model is justified and when simplified models suffice.
- Novel methodological integration of advanced PWA linearization techniques, specifically tailored for scenarios involving simultaneous optimization of battery sizing and operational scheduling. Unlike previous works that utilized fixed battery sizes to simplify battery degradation modelling, this study introduces an innovative approach to handle the nonlinearity arising from battery size-dependent state-of-charge calculations. This approach enables accurate modelling of both battery degradation dynamics and electrolyzer efficiency curves within the computationally manageable linear framework of MILP.
- Extension of rolling horizon optimization strategies to hybrid battery-hydrogen energy storage systems under real-time dynamic electricity pricing scenarios. This innovation significantly improves system adaptability, responsiveness, and operational feasibility, enabling better handling of renewable variability and demand fluctuations in practical applications.
- Integration of a multi-objective optimization framework, explicitly balancing economic objectives (LCOH minimization) with environmental goals (carbon emission intensity reduction). This dual-objective approach addresses a significant methodological gap, as previous studies often prioritized single-objective optimization without fully accounting for the inherent conflicts between economic and environmental targets, thus aligning this work with broader decarbonization and sustainability goals.
- Detailed and transparent methodological formulations and computational strategies, explicitly designed to ensure reproducibility, facilitate further methodological refinement, and support practical adoption by researchers and industry practitioners. This transparency greatly enhances the utility and applicability of the presented approaches, encouraging future adaptation in diverse scenarios, from industrial-scale hydrogen production to smaller-scale applications such as hydrogen refueling stations or domestic energy systems integrating fuel cells.

These contributions are validated through a comprehensive case study on an industrial-scale, grid-connected hydrogen production system. By explicitly incorporating realistic market conditions such as time-dependent electricity pricing, this work demonstrates how different optimization methods perform under conditions closely approximating actual industry operations.

Overall, this structured comparative framework provides practical insights and methodological innovations that substantially enhance the selection and deployment of suitable optimization strategies tailored specifically to complex, real-world renewable hydrogen production systems. Consequently, this study contributes significantly towards advancing methodological understanding, operational efficiency, and broader decarbonization efforts within sustainable energy systems.

The paper is organized as follows: Section 2 outlines the framework of the P2H system, detailing the data input and model configurations. Section 3 presents and discusses the results of the case study and

highlights the implications of different optimization approaches. Finally, Section 4 concludes the findings, and it offers insights into future research directions and practical applications.

2. Methods

2.1. Modeling framework and comparative setup

The power system investigated in this work consists of a green-hydrogen generation plant that features a proton exchange membrane (PEM) electrolysis stack. This system is powered by an on-site photovoltaic power plant, which was designed to meet the end-users' hydrogen demand. A battery energy storage system and a compressed hydrogen storage system were integrated to provide flexibility and ensure a consistent supply, despite the variability of the PV generation and hydrogen demand, thereby enhancing the exploitation of the renewable energy resources. In grid-connected scenarios, electric power can be withdrawn from the grid whenever there is a lack of PV generation, and any excess renewable power can be injected into the grid to boost the economic profitability of the plant. A schematic layout of the power-to-hydrogen system is shown in Fig. 1.

This modeling framework also introduces several methodological advances, including the adaptation of piecewise affine approximations for efficiency and degradation curves within a sizing context, and the implementation of a non-linear cycle-based degradation model in rule-based control, which enhances the realism and applicability of the proposed optimization strategies. Simulations were conducted over an entire year, considering an hourly time-step resolution, to compare different optimization models with varying levels of approximation for electrolyzer efficiency and battery degradation. The following scenarios were analyzed:

I. MILP_NL: a MILP model was used for both the sizing of the components and operational scheduling, with the efficiency of the electrolyzer and battery degradation being approximated with piecewise linear functions.
II. MILP_C: a MILP model was employed for sizing and scheduling purposes, assuming constant electrolyzer efficiency and linear battery degradation.
III. PSO_MILP_NL: a PSO model was applied for sizing purposes, while a MILP model with a rolling horizon optimization algorithm was used for scheduling. Piecewise linear functions were adopted for the efficiency of the electrolyzer and for the battery degradation curves.
IV. PSO_MILP_C: a PSO model was applied for sizing purposes, while a MILP model with a rolling horizon optimization algorithm was used for scheduling, and constant electrolyzer efficiency and linear battery degradation were assumed.
V. PSO_RB: a PSO model was adopted for sizing, along with a rule-based energy management strategy, in which non-linear functions were incorporated for electrolyzer efficiency and battery degradation.

The previous five scenarios were designed to systematically investigate the trade-offs between modeling fidelity, computational efficiency, and practical feasibility in both component sizing and operational scheduling. By varying the representation of key system dynamics, such as the efficiency of the electrolyzer and battery degradation (non-linear vs. constant/linear), and by testing different scheduling frameworks (single-horizon MILP, rolling horizon MILP or rule-based EMS), the analysis enables a clear quantification of the impact of each factor on the costs, emissions, and operational feasibility of the system. The inclusion of a rule-based EMS provides a computationally efficient and robust baseline that reflects realistic industrial implementations. This comparative framework supports the broader objective of identifying conditions under which a more sophisticated, higher-fidelity model would be justified and when a reduced-complexity formulation may offer sufficient accuracy at lower computational cost.

The hydrogen demand profile ($P_{H2,load}$) was derived from the final, natural-gas demand for industry reported in [46], and it was scaled to reflect the average, potential, hydrogen consumption in energy-intensive industrial processes, and to cover both high-temperature heat generation and feedstock needs. On the basis of data reported by Neuwirth et al. [47], a hydrogen consumption of 2 MWh per ton and a plant capacity of 100,000 tons per year were assumed (Fig. 2a). In addition to the hydrogen demand, the solar PV capacity factor profile, i.e. the ratio of the actual energy generated by the PV system (P_{PV}) over the installed nominal power, was integrated into the model to account

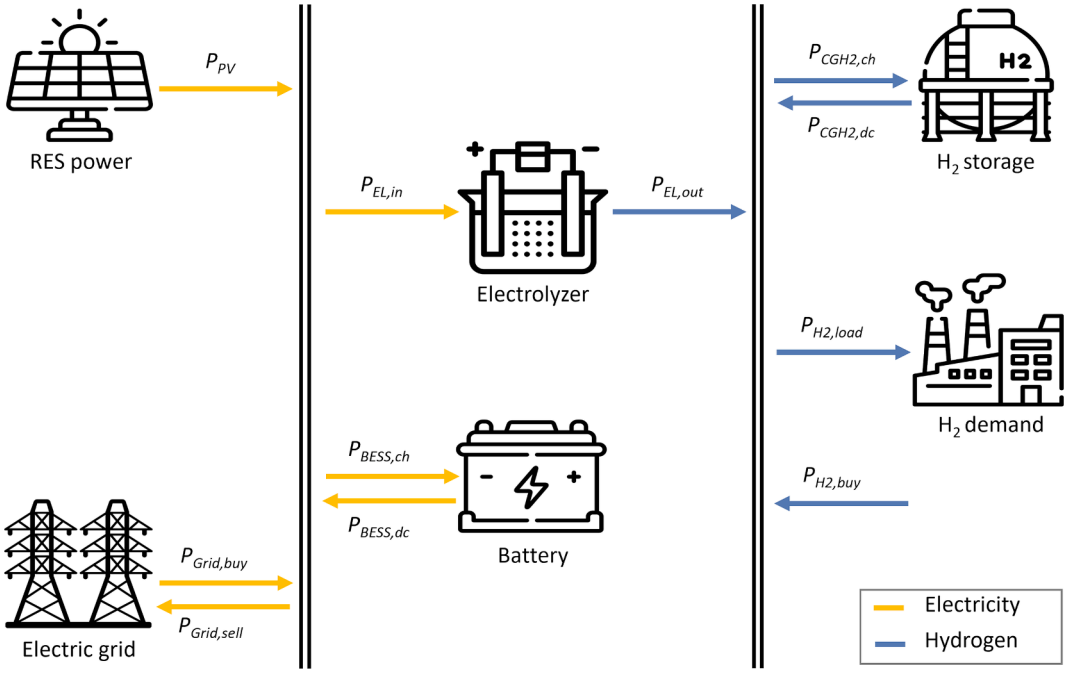

Fig. 1. Layout of the power-to-hydrogen system.

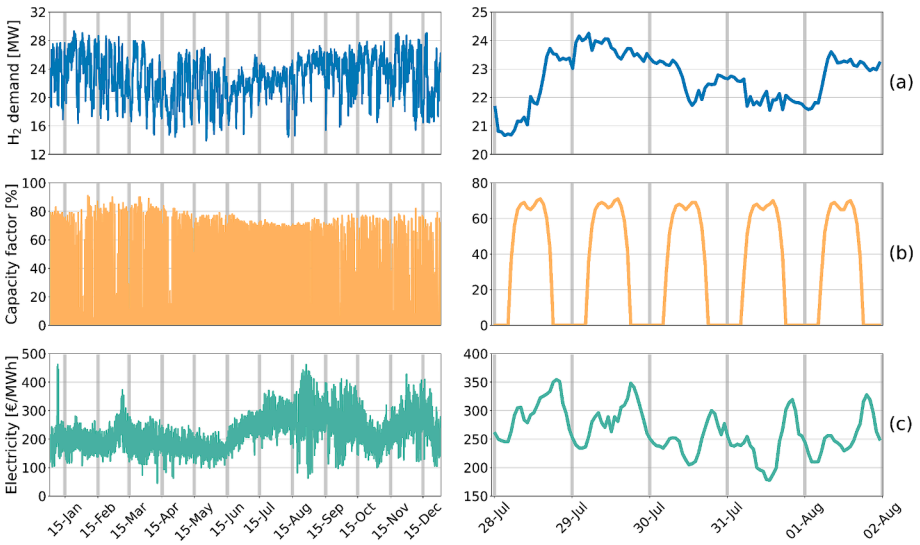

Fig. 2. Input data used for the model: a) hydrogen demand, (b) PV power capacity, and (c) electricity price. The left side shows the datasets for the entire year, while the right side presents the data profiles for a 5-day period.

for renewable energy production (Fig. 2b). This profile was obtained from the EU Photovoltaic Geographical Information System (PVGIS) [48] for a vertical axis tracking PV system with 14 % system loss, installed at a site in Italy. Finally, the average electricity price for the Italian market was calculated, to account for the cost variability of electricity withdrawn from the grid, by averaging the hourly profiles of the last 5 years (2019–2023), as sourced from the GME (Manager of the Energy Market) website [49]. These values were then adjusted by multiplying them by a factor of 1.7 to account for taxes and charges for industrial end-users, as reported by ARERA (Regulatory Authority for Energy Networks and the Environment) [50] (Fig. 2c).

The purpose of the objective function of the model (Eq. (1)) is to minimize the levelized cost of hydrogen within the P2H system (Eq. (2)), while simultaneously minimizing the carbon emission intensity (Eq. (5)). This optimization involves determining the optimal sizing of the system components and defining an EMS to dictate the production, storage, and energy delivery scheduling, thereby specifying the power consumption for each timestep.

$$f_{obj} = \min\left\{w_a \cdot f_{obj,a} + w_b \cdot f_{obj,b}\right\} \tag{1}$$

$$f_{obj,a} = \mathrm{LCOH} = \frac{\sum_{i,t}(C^{ann}_{inv,i}(t) + C_{O\&M}(t)_i - R(t))}{\sum H_2 demand(t)} \ [€/kg] \tag{2}$$

where C^{ann}_{inv} is the annualized capital cost of system component i, i.e. the equivalent annual cost of the capital investment, including both recovery of the initial expenditure (C_{inv}) and of the interest rate (r) over a specific payback period (n). This metric is calculated according to Eq. (3), using the capital recovery factor ($CRF(r,n)$) which spreads the cost of the investment over the useful lifetime of the components.

$$C^{ann}_{inv} = CRF(r,n) \cdot C_{inv} = \frac{r(1+r)^n}{(1+r)^n - 1} \cdot C_{inv} \left[\frac{€}{MW} or \frac{€}{MWh}\right] \tag{3}$$

The operation and maintenance costs ($C_{O\&M}$) encompass both fixed and variable expenditures. Fixed O&M costs include repairs and maintenance as well as component replacement. Variable O&M costs cover such utilities as electricity withdrawal and the purchase of hydrogen, which, in this case, was priced at 750 €/MWh. Additionally, revenues (R) can be derived from any surplus, renewable energy injected into the grid. The hydrogen selling price is calculated by adding 60 % to the green-hydrogen, levelized, production cost for Italy [51] to account for storage, transportation, taxes and profit margins. This approach discourages purchasing hydrogen in favor of on-site, hydrogen production.

The annualized value of all the replacement expenses (C^{ann}_{rep}) that occur over the lifetime of a project is calculated according to Eq. (4) [52,53].

$$C^{ann}_{rep} = SFF(r,y) \cdot C_{rep} \cdot F_{rep} = \frac{r}{(r+1)^y - 1} \cdot C_{rep} \cdot F_{rep} \left[\frac{€}{MW} or \frac{€}{MWh}\right] \tag{4}$$

where $SFF(r,y)$ represents the sinking fund factor, which is used to compute the future value of a series of equal annual cash flows, y is the lifetime of a component, and F_{rep} is the number of replacements required during the lifetime of the project.

The carbon emission intensity is calculated according to Eq. (5).

$$f_{obj,b} = \sum_t P_{Grid,buy}(t) \cdot I_{CO_2} \ [kt_{CO2}/yr] \tag{5}$$

where $P_{Grid,buy}$ represents the amount of energy withdrawn from the electric grid, I_{CO_2} is the average carbon emission intensity in Europe, which is set to 250 g_{CO2}/kWh [54], and the scalar coefficients w_a and w_b represent the weighting factors used in the weighted sum method to balance the two objectives [55].

The main techno-economic data assumed as model input parameters are summarized in Table 1.

The electrolyzer system efficiency (η_{EL}) is evaluated according to Eq. (6).

$$\eta_{EL} = \frac{P_{EL,out}}{P_{EL,in} + P_{EL,aux}} = \frac{n_{H2} \cdot LHV_{H2}}{P_{EL,in} + 0.1 \cdot P_{EL,in}} \ [\%] \tag{6}$$

Where $P_{EL,in}$,$P_{EL,out}$ and $P_{EL,aux}$ represent the electrolyzer input, output, and auxiliary power, respectively. n_{H2} is the number of moles of hydrogen generated while accounting for Faraday (or parasitic) current losses, and LHV_{H2} is the lower heating value of hydrogen. The term $0.1 \bullet P_{EL,in}$ accounts for the auxiliary energy demand for fans, pumps, cooling, and control systems, which is set to 10 % of the electrolyzer power consumption [63]. $P_{EL,in}$ and n_{H2} are evaluated according to the current–voltage characteristics of the electrolyzer, which were derived from the polarization curve described by Rozzi et al. [60]. Further details on the parameters involved in this equation can be found in Section S.1 of the Supplementary Material.

The BESS degradation curve resulting from aging is computed using an empirical degradation function, adapted from the work of Grimaldi et al. [61]. A ninth-order polynomial equation has been adopted to

Table 1
Techno-economic parameters used for the P2H model.

Parameter	Value	Reference
PV system		
CAPEX	1200 €/kW*	Utility-scale, one-axis, tracking systems [56]
OPEX	2 %	Utility-scale, one-axis, tracking systems [56]
Lifetime	Project lifetime	
Capacity bounds	0–200 MW	
Electrolyzer		
CAPEX	900 €/kW	100 MW electrolyzer [57] + 10 % installation costs [58,59]
OPEX	3 %	[57]
Replacement cost	40 %	[57]
Stack lifetime	10 y	[57]
Lifetime BOP	Project lifetime	
Operating range	5–100 % of nominal power	[60]
Efficiency	Efficiency curve Constant: 62.5 %	Based on the polarization curve model [60]
Capacity bounds	0–200 MW	
Hydrogen storage		
CAPEX	10 €/kWh	[57]
OPEX	2 %	[57]
Lifetime	Project lifetime	
Operating range	10–100 %**	
Initial state-of-fill	50 %	
Capacity bounds	0–200 MWh	
Battery energy storage system		
CAPEX	300 €/kWh + 150 €/kW	Battery with a 200 MWh/50 MW energy capacity [57]
OPEX	2 %	[57]
Replacement costs	50 %	[57]
Module lifetime	7000 cycles	End of life 65 %, obtained on the basis of the degradation curve [61]
Lifetime BOP	Project lifetime	
Operating range	15–95 % of the nominal capacity	[54]
Initial state-of-charge	50 %	
Efficiency	Battery efficiency:93 % Inverter efficiency: 96 %	[57,61]
Self-discharging	0.008 %/h	[56]
Degradation	Degradation curve Linear:$1-5.02\,10^{-5}\,cyc$	[61]
Capacity bounds	0–200 MWh	
Other economic parameters		
Electricity purchase price	Hourly data	[49,50]
Electricity selling price	40 % of the hourly electricity price	[62]
Discount rate	5 %	[54]
Project lifetime	20 y	[62]
Hydrogen purchase cost	750 €/MWh	[51]

* Exchange rate: 1 USD = 0.92 EUR.
** The hydrogen storage system operates at a maximum pressure of 30 bar, which is the output pressure of the electrolyzer. Moreover, the pressure requirement for the end-user is set at 3 bar.

accurately represent the remaining capacity as a percentage of the initial capacity ($SOC_{BESS,rem}$), and as a function of the number of cycles (cyc) performed by the battery (Eq. (7)).

$$SOC_{BESS,rem} = 100 - 5.613^{-32}\cdot cyc^{9} + 3.121^{-27}\cdot cyc^{8} - 6.353^{-23}\cdot cyc^{7} + 6.630^{-19}\cdot cyc^{6} - 3.987^{-15}\cdot cyc^{5} + 1.435^{-11}\cdot cyc^{4} - 3.070^{-8}\cdot cyc^{3} + 3.746^{-5}\cdot cyc^{2} - 0.0277\cdot cyc\ [\%] \quad (7)$$

The output variables returned by the models include both design and operational parameters, which are crucial for defining the performance of the P2H system.

The design parameters specify the sizes of the system components, including the nominal power of the PV system ($P_{PV,nom}$), BESS ($P_{BESS,nom}$), and the electrolyzer ($P_{EL,nom}$), as well as the nominal energy capacity of BESS ($E_{BESS,nom}$) and the CGH_2 system ($E_{CGH_2,nom}$). Each of these design variables is constrained to a maximum of 200 MW (for power ratings) or 200 MWh (for energy capacities).

The operational parameters describe the energy management strategy, i.e. the operational scheduling computed for each timestep of the simulation period, and they include the following:

i. The input power to the electrolyzer ($P_{EL,in}$) and the output power generated by the electrolyzer ($P_{EL,out}$)
ii. The power exchanged with the BESS, that is, both charged and discharged ($P_{BESS,ch}, P_{BESS,dc}$)
iii. The energy stored in the BESS ($E_{BESS,stored}$)
iv. The remaining energy capacity of BESS ($E_{BESS,rem}$)
v. The hydrogen exchanged with the hydrogen storage system, both charged and discharged ($P_{CGH_2,ch}, P_{CGH_2,dc}$)
vi. The hydrogen stored in the CGH_2 system ($E_{CGH_2,stored}$)
vii. The power exchanged with the electric grid, including both withdrawal and injection ($P_{Grid,buy}, P_{Grid,sell}$)
viii. The purchased hydrogen ($P_{H2,buy}$)

2.2. MILP modeling and optimization

The model was developed in the Python environment using the Pyomo framework [64], and was solved using the Gurobi™ solver [65]. The computations were performed on a workstation equipped with an Intel(R) Core(TM) i7-10700 K CPU and 32 GB of RAM. The maximum allowable relative MIP gap tolerance was set at 1%. The model utilized parallel processing across 16 threads, with a specified Cuts level set to 3. Additionally, a time limit of 48 h was imposed, and the No Relaxation heuristic parameter (NoRelHeurWork), which specifies the maximum time elapse between two iterations of the heuristic process, was set to 1000 s.

As shown in Fig. 1, the system is denoted by two nodes: one for the exchange of electric power and one for balancing the hydrogen energy. The electric power exchange node manages the flows of electric power generation and consumption (Eq. (8)), while the hydrogen energy balance node oversees hydrogen production, storage, and consumption (Eq. (9)). These power balances should be satisfied simultaneously at each time step.

$$P_{PV}(t) + P_{BESS,dc}(t) + P_{Grid,buy}(t) = P_{EL,in}(t) + P_{BESS,ch}(t) + P_{Grid,sell}(t)[MW] \quad (8)$$

$$P_{EL,out}(t) + P_{CGH_2,dc}(t) + P_{H2,buy}(t) = P_{CGH_2,ch}(t) + P_{H2,load}(t)[MW] \quad (9)$$

A detailed formulation of the MILP model, including all component-specific constraints and the objective function, is presented in Section S.2 of the Supplementary Material.

2.2.1. 2.2.1Piecewise functions

The non-linear behavior of the efficiency of the electrolyzer in the MILP problem and the BESS degradation curves were modeled by introducing piecewise affine (PWA) linearization functions. This approach approximates non-linear curves in linear segments. The method proposed by Marocco et al. [41] was employed for the efficiency of the electrolyzer. In this method, the normalized output power ($\eta_{EL}\cdot P_{EL,in}/P_{EL,nom}$) is computed as a function of the normalized input power ($P_{EL,in}/P_{EL,nom}$). As can be seen in Fig. 3a, this curve is divided into three linear segments defined by four breakpoints. Fig. 3b illustrates the resulting efficiency curve after the PWA linearization of the power

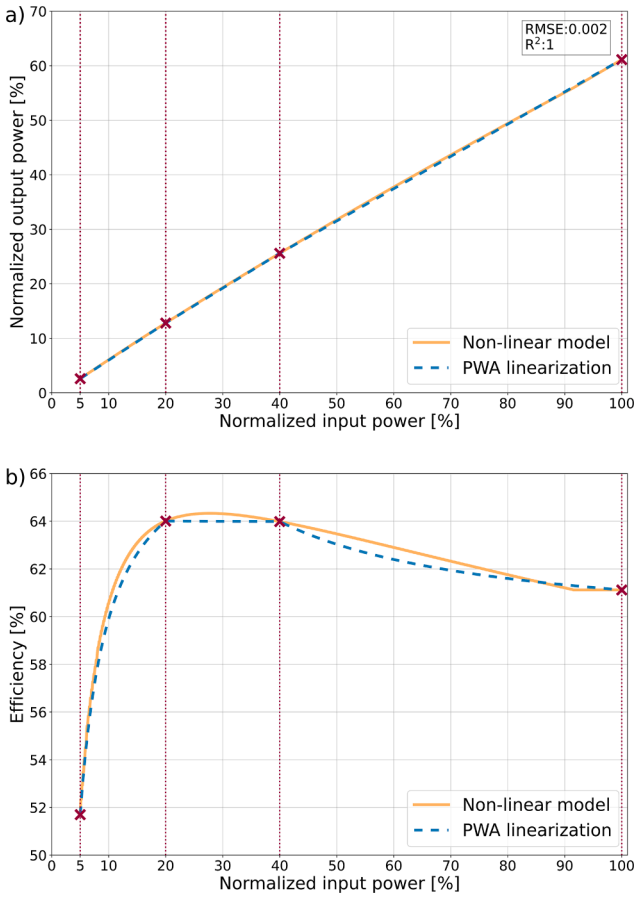

Fig. 3. Non-linear model and PWA linearization of the efficiency of the electrolyzer: a) normalized output power as a function of the normalized input power, b) efficiency of the electrolyzer as a function of the normalized input power. The markers indicate the breakpoints of the PWA segments.

output curve.

A similar approach was applied to the BESS degradation curve. The remaining capacity is described as a function of the number of cycles, by three linear segments defined by four breakpoints (Fig. 4).

The number of breakpoints is a balance between the approximation error (root mean square error) and increased computational time. The quality of the fit was evaluated by computing the root mean square error (RMSE) and the coefficient of determination (R^2). For the battery degradation curve, the linear approximation resulted in an RMSE of 2.79 % and an R^2 of 0.89, while the PWA model significantly improved the fit, achieving an RMSE of 0.52 % and an R^2 of 0.996. For the electrolyzer efficiency curve, the PWA approximation yielded an RMSE of 0.16 % and an R^2 greater than 0.999, indicating an excellent correspondence with the original non-linear profile. In contrast, assuming a contrast electrolyzer efficiency of 62.5 % results in a significantly higher RMSE of approximately 1.77 %. Nonetheless, this constant efficiency value was selected as it represents a typical average efficiency for commercially available electrolyzers [57]. These results confirm the high accuracy of the PWA approach, particularly when compared to simpler linear representations. Additional details on the PWA linearization are presented in Section S.3 of the Supplementary Material.

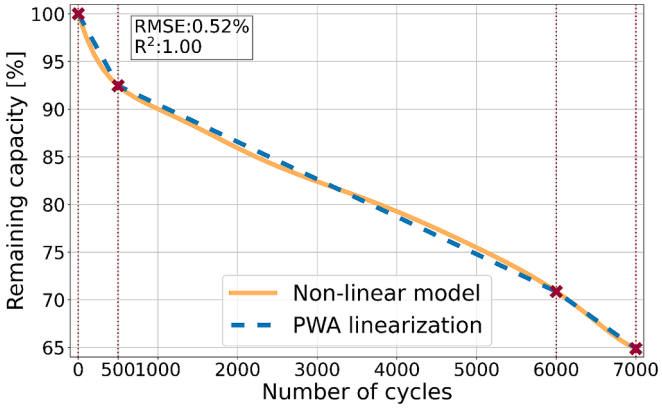

Fig. 4. Non-linear model and PWA linearization of the BESS degradation curve. The markers indicate the breakpoints of the PWA segments.

2.2.2. *Rolling horizon*

The rolling horizon approach allows a continuous re-optimization to be made by dividing the simulation period into smaller intervals and repeatedly solving the optimization problem over a shifting time window (optimization horizon *H*). Initially, optimization horizon *H* is chosen, and a size *U* step, which determines the extent of the shift for each iteration (update interval), is set. The optimization problem is solved for the current optimization horizon, *H*, using the latest available data. This involves determining the optimal scheduling and dispatching of resources within the optimization horizon. The first part of the solution, which covers *U* hours, is implemented and saved as the problem solution. The optimization horizon is then moved forward by the size *U*step, and the system state is updated with the most recent data. The optimization process is again repeated for the new optimization horizon until the final scheduling period is reached.

Fig. 5 illustrates the scheduling mechanism for the rolling time horizon approach with an optimization horizon of 48 h and a step size of 24 h. A 24-hour update period is selected to capture the cyclic nature of

the PV systems, while a 48-hour optimization horizon is considered to account for next-day effects, while avoiding the excessive computational time associated with longer horizons [40].

The rolling horizon approach, which breaks down the optimization period into smaller intervals, is unsuitable for optimizing such design variables as the size of system components. This is because it focuses on short-term decisions within each time window, thereby preventing the adjustment of design variables across different horizons. For this reason, a two-layer optimization strategy is implemented. In this approach, PSO is used to optimize the component sizes (design variables), while MILP handles the operational scheduling (Fig. 6). Details on the PSO algorithm implementation are reported in Section 2.2.

2.3. PSO modeling and optimization

The particle swarm optimization algorithm is a stochastic *meta*-heuristic technique that is implemented in Python using the pyswarms framework [66]. PSO seeks the global optimum by iteratively refining candidate solutions, which are represented as particles. These particles, which are influenced by their individual experiences (cognitive behavior) and the collective influence of their neighbors (social behavior), explore the search space. The algorithm adjusts the velocity and position of each particle according to Eq. (10) and Eq. (11), and thus drives the swarm toward an optimal solution.

$$v_{ij}(k+1) = w \cdot v_{ij}(k) + c_1 \cdot r_{1j}(k) \cdot \left[y_{ij}(k) - x_{ij}(k) \right] + c_2 \cdot r_{2j}(k) \cdot \left[\hat{y}_j(k) - x_{ij}(k) \right] \quad (10)$$

$$x_{ij}(k+1) = x_{ij}(k) + v_{ij}(k+1) \quad (11)$$

where the subscript i refers to a specific particle in the swarm, j indicates a specific dimension in the search space, and k represents the iteration. The hyperparameters w, c_1 and c_2 control the momentum of the particles, and they balance the exploration (searching new areas) and exploitation (refining the current best solutions); w influences the inertia of the particles and impacts their tendency to continue in their current direction; c_1 affects the cognitive behavior and guides the particles toward their individual, best-known positions; c_2 influences the social behavior and directs particles toward the global best-known position discovered by the swarm. The $x_{ij}(k+1)$ position is updated by adding a new velocity, $v_{ij}(k+1)$, to the current position, $x_{ij}(k)$. The new velocity is computed on the basis of the previous velocity of the particle, $v_{ij}(k)$, the cognitive component influenced by the individual best position of the particle, $y_{ij}(k)$, and the social component influenced by the global best position, $\hat{y}_j(t)$. The random values $r_{1j}(k)$ and $r_{2j}(k)$, which are uniformly distributed between 0 and 1, introduce stochastic behavior into the particle paths.

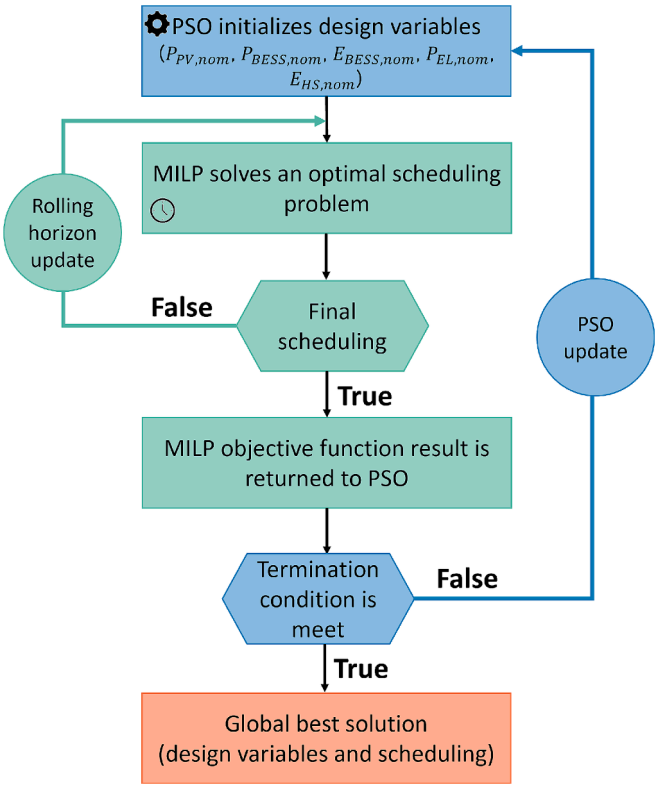

Fig. 6. Schematic of the two-layer, optimization framework that combines PSO for design optimization and MILP with a rolling horizon for operational scheduling.

In this study, the problem search space consisted of 5 dimensions, which corresponded to the design variables that had to be optimized. The PSO algorithm parameters – including population size (number of particles), number of iterations, inertia weight (w), and cognitive (c_1) and social (c_2) acceleration coefficients – were carefully selected based on a systematic analysis conducted through a structured grid search approach. The optimal parameter selection considered multiple criteria simultaneously: the quality of the obtained solution (best objective function value), computational time required for convergence, and practical feasibility of the resulting solutions. The complete set of PSO parameters explored in the grid search, along with the corresponding tested ranges and the final selected optimal settings, are summarized in Table B1. A linear adjustment of the acceleration coefficients and inertia weight facilitates a gradual shift from exploration to exploitation, and it enhances the convergence of the algorithm while preserving the

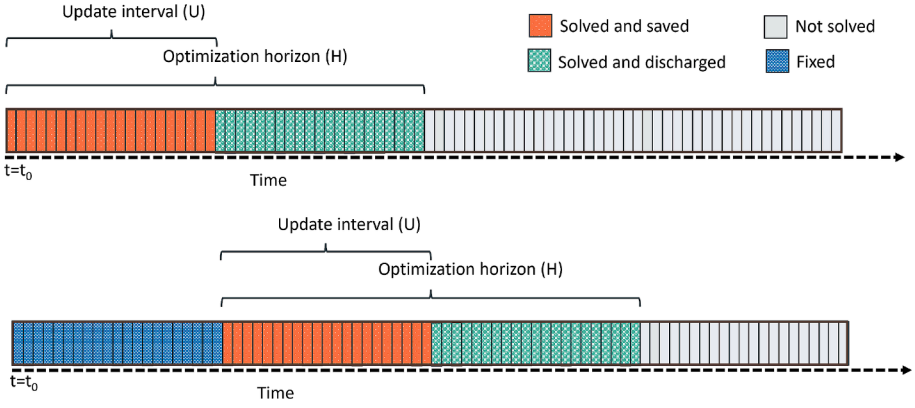

Fig. 5. Schematic diagram of the rolling horizon model.

exploration of a solution in the early iterations. The search space was bounded by design variable limits, ranging from 0 to 200 MW (or MWh).

In the specific case of the PSO_RB configuration, the optimization process is coupled with a rule-based energy management strategy, rather than an embedded scheduling model. At each time step, the model updates the relevant state variables to track the available renewable energy, the energy directed toward storage, and the energy used to meet the load demand. The core of the simulation logic revolves around allocating the available renewable energy, while focusing on whether the hydrogen load can be met directly by power from the electrolyzer or whether hydrogen needs to be drawn from storage.

When the hydrogen load is positive, the model checks if it can be satisfied by the power made available by the electrolyzer. If so, it calculates the power delivered to the electrolyzer, updates the energy storage levels, and determines any excess renewable energy. If the hydrogen load is not met fully by direct production, the model attempts to supplement it with stored hydrogen. When the stored hydrogen is insufficient to meet the demand, additional hydrogen is purchased. The system prioritizes powering the electrolyzer with PV energy, and any additional required energy is supplied by the battery. If the battery capacity is insufficient, the remaining energy is drawn from the grid. After meeting the load requirements, any excess energy is stored in available storage devices (battery or hydrogen storage). When these storage devices are at full capacity, any excess PV electricity is sent to the grid. The electrolyzer efficiency and battery degradation are both modeled according to the non-linear functions presented above. The complete schematic of the flowchart for this model is detailed in Section S.4 of the Supplementary Material.

2.4. Performance indicators

Certain key performance indicators (KPI) were introduced to compare the proposed models: four design indices and three scheduling indices. The design indices include the import index, which measures the ratio of electricity purchased from the grid to the total load, calculating according to Eq. (12).

$$ImportIndex = \frac{\sum P_{Grid,buy}(t)}{\sum P_{H2,load}(t)}\ [\%] \tag{12}$$

The PV surplus index evaluates the proportion of surplus energy generated by the PV panels that is injected into the grid, as repS.5resented by Eq. (13).

$$PV_{surplus} = \frac{\sum P_{Grid,sell}(t)}{\sum P_{PV}(t)}[\%] \tag{13}$$

Additionally, the storage utilization factors indicate the ratio of energy consumed from the battery, or the hydrogen storage, to their nominal capacity, defined as per Eq. (14) and Eq. (15).

$$BESSutilization = \frac{\sum P_{BESS,dc}(t)\cdot\Delta t}{E_{BESS,nom}}\ [\%] \tag{14}$$

$$CGH_2utilization = \frac{\sum P_{CGH_2,dc}(t)\cdot\Delta t}{E_{CGH_2,nom}}[\%] \tag{15}$$

Instead, the scheduling indices consist of the average state of charge or state of fill ($SOC_{BESS,ave}, SOF_{CGH_2,ave}$), which reflects the average charge level of the storage systems over time (Eqs. (16)–(17)), and the average efficiency of the electrolyzer ($\eta_{EL,ave}$), which indicates the average efficiency achieved during its operation (Eq. (18)).

$$SOC_{BESS,ave} = mean\left(\frac{E_{BESS,stored}(t)}{E_{BESS,nom}}\right)[\%] \tag{16}$$

$$SOF_{CGH_2,ave} = mean\left(\frac{E_{CGH_2,stored}(t)}{E_{CGH_2,nom}}\right)[\%] \tag{17}$$

$$\eta_{EL,ave} = mean(\eta_{EL}(t))[\%] \tag{18}$$

3. Results

The results of the comparative assessment of the optimization algorithms used for the design and operational management of the P2H system are presented in the following sections. The analyzed models are summarized in Table 3. The optimization variables, along with the techno-economic input parameters and constraints applied in the modeling framework, are detailed in Section 2.1 and Table 1.

The objective function of this optimization problem attempts to minimize both the levelized cost of hydrogen and carbon emissions. Fig. 7 presents the outcomes obtained for the objective function for the algorithms, while Fig. 8 illustrates the component sizing and electricity exchanges with the grid, including imports and exports.

The comparative analysis revealed significant differences in the optimization outcomes, component sizing, and grid reliance of the different models. The PSO_RB model, which used a rule-based energy management strategy, achieved the lowest level of CO_2 emissions (14.3 kt/y), which resulted in a 27–45 % reduction, compared to the other models. This outcome largely resulted from its minimized grid imports (57 GWh), as the rule-based approach only drew power from the grid when no other energy source was available. However, this strategy led to an 8–26 % increase in LCOH. The higher LCOH was attributed to the need for a larger battery power rate (94 MW) to maintain system autonomy, together with a 20 % increase in PV capacity (196 MW) and a 70 % increase in battery cycles, compared to the MILP_C model. This heavy reliance on PV and battery storage raised the investment and operational costs relative to battery degradation, thereby impacting LCOH.

The MILP_NL and MILP_C models, which employed mixed-integer linear programming for both sizing and scheduling, adopted a different approach that involved depending more heavily on grid imports (103 GWh and 84 GWh, respectively). This reduced their PV requirements and grid exports (91 GWh and 100 GWh, respectively). MILP_NL operated with a PV capacity of 150 MW and a 49 MW battery power rate, while MILP_C relied on a slightly larger PV system (165 MW) and a substantially higher power rating (127 MW). Both models employed the maximum available hydrogen and battery storage energy capacity (200 MWh), with electrolyzer sizes of 150 MW for MILP_NL and 200 MW for MILP_C. Although this strategy lowered the need for internal energy resources, the increased grid dependence resulted in 32–45 % higher CO_2 emissions than PSO_RB, thus making these models less environmentally favorable. It should be noted that, despite the objective function having been defined to minimize both the LCOH and CO_2 emissions, these models prioritized an LCOH reduction at the expense of increased CO_2 emissions. As a result, the rule-based PSO_RB model performed better, in terms of environmental impact, thereby highlighting the trade-offs inherent to the optimization objectives of the MILP models.

The PSO_MILP_NL and PSO_MILP_C models, which combined particle swarm optimization for sizing with MILP and rolling horizon optimization for scheduling, provided a more balanced approach. These models showed moderate grid imports (79 GWh and 81 GWh, respectively) and significantly higher grid exports (153 GWh and 122 GWh) than the MILP-only models, and this contributed to lowering CO_2 emissions and achieving higher revenues from electricity sales. These models, which optimized PV capacities of 179 MW and 197 MW, respectively, reduced dependency on the grid, without the need for oversized battery storage capacities, which remained at 168 MWh and 134 MWh with minimal power ratings (10 MW and 9 MW). This strategy achieved a 9–14 % reduction in LCOH, compared to the MILP_NL and MILP_C models. The rolling horizon optimization facilitated an efficient use of the resources, and a balancing of the costs and emissions, without an excessive reliance on grid power or oversized storage solutions.

Table 3
Optimization strategy, electrolyzer efficiency, and battery degradation assumptions of the five case studies.

Case	Name	Optimization strategy adopted for component sizing	Optimization strategy adopted for operational scheduling	Electrolyzer efficiency	Battery degradation
1	MILP_NL	MILP[a]	MILP	Piecewise linear function	Piecewise linear function
2	MILP_C	MILP	MILP	Constant	Linear function
3	PSO_MILP_NL	PSO[b]	MILP	Piecewise linear function	Piecewise linear function
4	PSO_MILP_C	PSO	MILP	Constant	Linear function
5	PSO_RB	PSO	RB[c]	Non-linear function	Non-linear function

[a] MILP: mixed-integer linear programming.
[b] PSO: particle swarm optimization
[c] RB: rule-based energy management strategy.

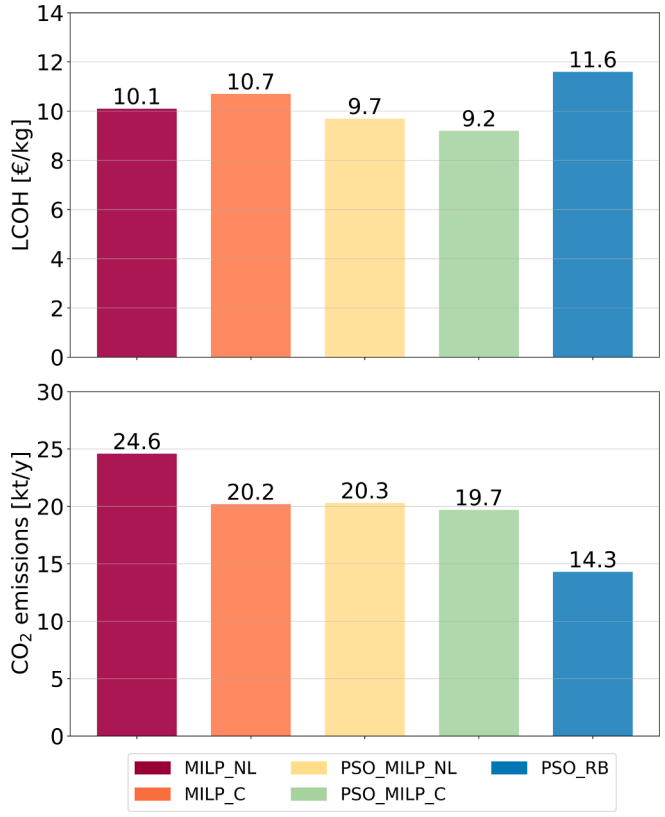

Fig. 7. Objective function metrics: levelized cost of hydrogen (LCOH) and CO_2 emissions.

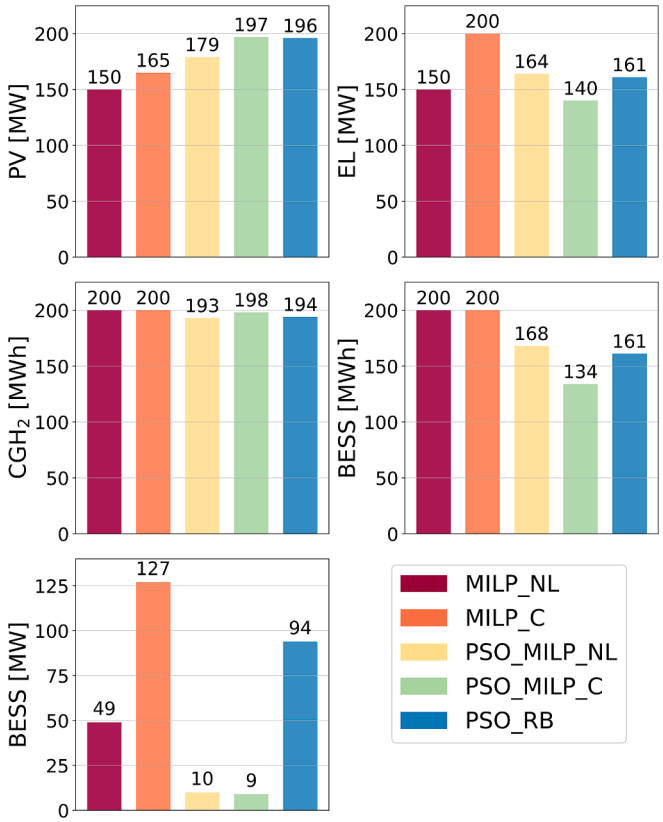

Fig. 8. Component size for the different models.

Fig. 9 summarizes the results of the import and PV surplus indicators for analyzed models.

An analysis of the Import Index and PV surplus values provided further insights into the reliance of each model on the grid and the efficiency of the utilization of renewable energy. As can be observed in the figure, the PSO_RB model, which has the lowest Import Index, that is, 29 %, demonstrates the lowest dependence on grid imports, consistent with its minimized grid reliance (57 GWh), and the lowest CO_2 emissions. This reduced Import Index is coupled with a moderate PV surplus of 31 %, thus suggesting an effective management of the excess solar generation to meet the demand, without any significant overproduction. Instead, the MILP_NL model exhibits the highest Import Index, that is, 49 %, thereby reflecting a greater dependency on grid power (100 GWh). Despite this, its PV surplus remains similar to that of PSO_RB, which is at 31 %, thus suggesting that much of the generated PV power is either directly utilized or stored. The other models fall within an Import Index range of 40 % and 41 %, with PV surplus values varying from 29 % for MILP_C to 37 % for PSO_MILP_C.

Fig. 10 shows the key performance indicators for hydrogen and battery energy storage.

The BESS and CGH_2 utilization metrics reveal the extent of battery and hydrogen storage usage across the models. As can be seen in Fig. 10, the PSO_RB model has the highest BESS utilization with 173 cycles, which would seem to indicate an intensive battery use, due to its low grid dependence. Instead, MILP_NL shows a significantly lower BESS utilization, with only 16 cycles, which is aligned with its heavy reliance on grid imports and limited battery power (49 MW). This low utilization suggests that 200 MWh BESS is an inefficient solution, as it does not justify the capital expenditure. The PSO_MILP_C and PSO_MILP_NL models achieve intermediate BESS utilization levels of 162 and 140 cycles, respectively, thereby striking a balance between grid reliance and storage use, without the excessive cycling that would increase operational costs. Despite the potential for a higher utilization, the significant costs associated with battery degradation and the option of utilizing hydrogen storage contribute to the underutilization of the battery system.

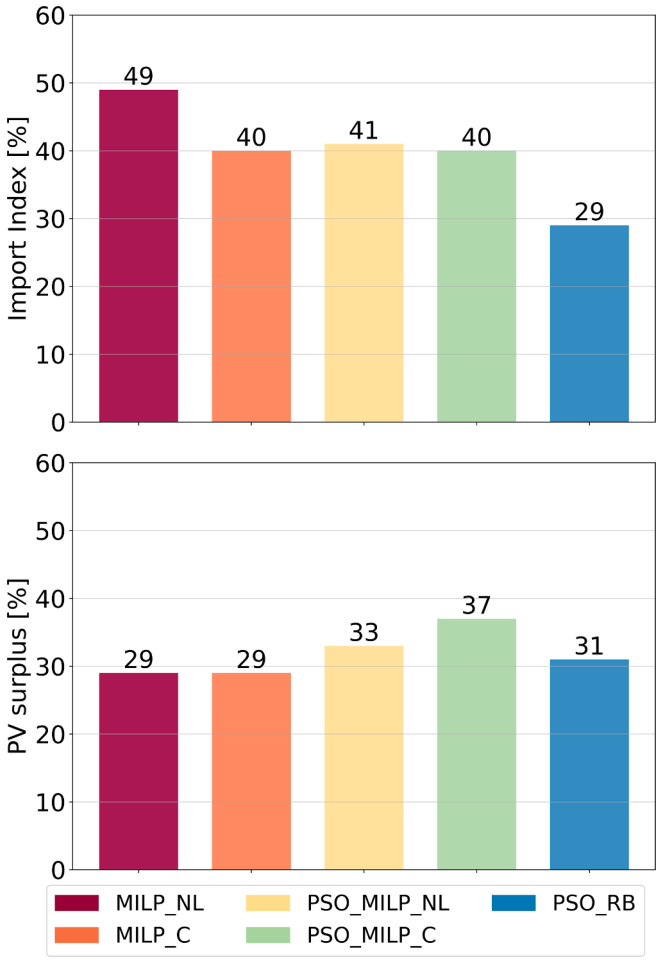

Fig. 9. Performance index of the imports and PV surplus.

In terms of CGH_2 utilization, PSO_MILP_C exhibits the highest hydrogen storage usage with 423 cycles, while the PSO_RB and MILP_NL models show lower utilization levels with 297 cycles. This difference reflects the trade-off between battery and hydrogen storage as energy buffers. PSO_MILP_C achieves a higher CGH_2 utilization by optimizing both storage and dispatching, thereby reducing grid dependency while efficiently using hydrogen as an alternative storage medium. Moreover, its higher utilization in MILP_C and PSO_MILP_C could also be partially attributed to the efficiency of the electrolyzer. Models that demonstrate greater hydrogen storage utilization typically exhibit more consistent and higher efficiency than other MILP models. This enhanced efficiency enables a better conversion of excess renewable energy into hydrogen, thereby further optimizing the overall energy management strategy.

The remaining BESS capacity also varies for the different models. Degradation in the MILP_NL and MILP_C models is only calculated on the basis of the cycle count, without considering the SOC levels. As a result, even though the BESS utilization in the MILP_NL model is only 16 cycles, the remaining capacity is calculated considering partial cycles (103 for MILP_NL and 334 for MILP_C), thus leading to a lower remaining capacity than what is utilized. Moreover, the models that employ linear degradation functions, such as MILP_C and PSO_MILP_C, may underestimate the initial steep degradation curve, and this results in a slight overestimation of the capacity remaining after one year. This simplification is reflected in their relatively high remaining capacities (0.983 and 0.990, respectively) compared to what could be expected for an equivalent number of cycles using non-linear degradation functions. For instance, although the cycle counts of the PSO_RB model (173 cycles) and PSO_MILP_C model (162 cycles) are similar, the remaining

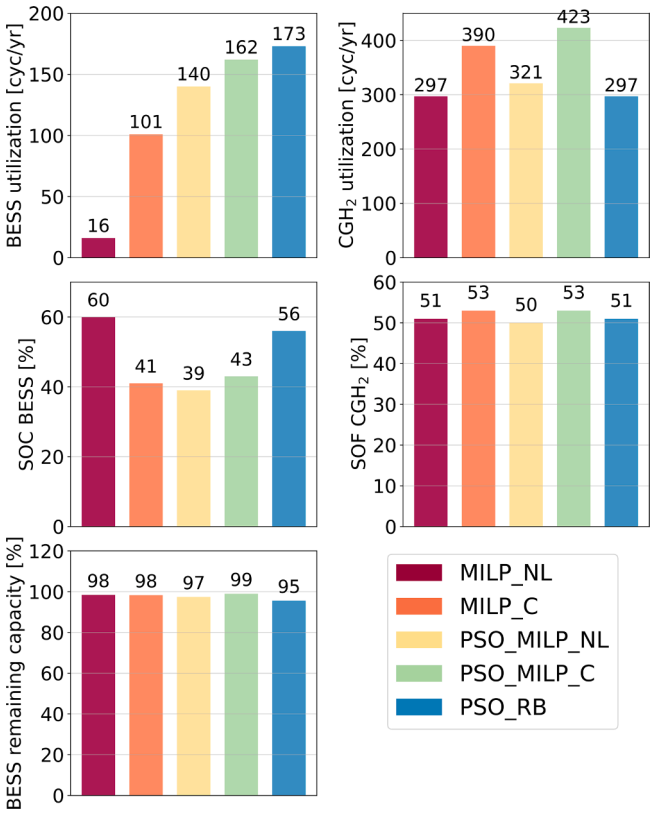

Fig. 10. Performance indicators of the hydrogen and battery energy storage.

BESS capacity in the PSO_RB model is only 0.956 lower than the 0.99 of the PSO_MILP_C model. However, it is important to note that this reduction in battery capacity has less impact than the financial implications of degradation costs.

Finally, the state of charge of BESS and the state-of-fill of CGH_2 illustrate the average utilization levels of each storage type. PSO_RB shows the highest average SOC for BESS (56 %), thereby indicating a preference for maintaining higher energy reserves in the battery, due to its rule-based strategy, which minimizes grid imports. MILP_NL, with a high grid dependency, operates with a moderately high SOC of 60 % for BESS, but it shows a relatively low BESS utilization, thus suggesting that, although energy is stored, it is less frequently cycled. The SOF for CGH_2 remains consistent across most of the models, hovering around 50–53 %, with PSO_MILP_C and MILP_C utilizing a slightly higher fill level, which is aligned with their higher CGH_2 usage.

An analysis of the electrolyzer efficiency revealed that the PSO_RB model achieved the highest average electrolyzer efficiency, that is, 63.6 %. This is primarily because it operated closer to the nominal power more frequently than the other models, thanks to its rule-based strategy, which prioritized electrolyzer utilization. Consequently, the PSO_RB model demonstrated a more stable and efficient use of the electrolyzer over time. On the other hand, the MILP_NL and PSO_MILP_C models exhibited a lower average electrolyzer efficiency, that is, of around 60 %, thus indicating that their operational conditions were not consistently optimal, and this resulted in a less effective performance than the PSO_RB model.

Fig. 11 and Fig. 12 illustrate the electrical and hydrogen energy balances of the different models. Positive values represent power supply variables (red line), including RES power production (bright yellow fill), battery discharge power (dark yellow fill), and grid withdrawal power (orange fill). Conversely, negative values correspond to power demand variables (dark blue line), such as electrolyzer power (light blue fill), battery charge power (teal fill), and grid-injected power (light cyan fill). Section A in Fig. 11 highlights the various strategies that can be adopted

to manage the electricity demand when PV production is absent. In the MILP_and PSO_MILP_models, the electrolyzer operates continuously at different power levels, that is, it adapts to the available energy. However, the battery is rarely used in the MILP_NL and MILP_C models, as can be deduced from previous results, and this leads to a greater reliance on grid imports to satisfy the demand. The PSO_MILP_NL and PSO_MILP_C models instead show a clear preference for battery usage, whenever it is available; these models only resort to the grid to cover peak loads when the BESS state of charge reaches its minimum. The PSO_RB model adopts yet another approach: in the hours leading up to PV production, the battery is discharged to meet the demand, while after PV production, hydrogen storage – charged during PV generation – is used to satisfy the energy needs. It should be noted that this model avoids grid imports completely during these periods and relies solely on internally stored resources.

Section B in Fig. 11 further emphasizes the distribution of PV energy between the electrolyzer, battery charging, and grid exports. In the MILP_NL and MILP_C models, PV energy is primarily shared between powering the electrolyzer and injecting any surplus into the grid, with minimal battery charging. The PSO_MILP_NL, PSO_MILP_C, and PSO_RB models instead allocate a portion of surplus PV energy to battery charging. The PSO_MILP_NL model, in which electrolyzer efficiency is affected by the operating point, tends to operate the electrolyzer close to its nominal capacity, albeit for shorter periods. On the other hand, PSO_MILP_C does not account for power-dependent efficiency for hydrogen production, and this results in a steadier operation for less power. The electrolyzer in the PSO_RB model initially operates at nominal power, until the compressed hydrogen storage reaches full capacity, and it then adjusts to meet the demand as needed, as demonstrated in Fig. 12.

As far as the hydrogen balance in Fig. 12 is concerned, section A reveals a notable difference in hydrogen load coverage among the models. The PSO_RB model emerges as the only model that is capable of meeting the hydrogen demand solely from CGH_2 stored during periods without PV production. The other models instead mainly rely on hydrogen storage, but part of their demand is still supplied by the electrolyzer, which operates at minimal power, thereby leading to reduced efficiency.

Fig. 12 also illustrates how the operation of the electrolyzer is affected by the state of filling of hydrogen storage. Section B reflects the patterns that were observed in the electrical energy balance. A distinctive feature of the PSO_RB model is that hydrogen storage is charged at the start of PV production and remains fully charged throughout the PV generation period, only to be fully discharged during non-solar hours. Instead, hydrogen storage typically charges more gradually in the other models, often reaching a partial peak halfway through PV production, due to temporary drops in the PV output, before completing the charge cycle later on during the day.

In addition to energy, economic and environmental performance, the computational efficiency of each optimization strategy was assessed. The MILP-based models required up to 48 h to return results, with MIPGap values remaining above 30 % in complex scenarios. The hybrid PSO-MILP models achieved convergence within 27–35 h with MIPGap values below 1 %, thanks to the use of a rolling horizon approach. The PSO_RB model, relying on rule-based control, completed its optimization in only 1.5 h. These findings underscore the importance of balancing solution quality with computational feasibility, particularly in applications where scalability and response time are critical.

4. Discussion

This section discusses the broader implications of the results by analyzing how different optimization strategies and modeling choices influence system performance. Special attention is given to the trade-offs between cost, emissions, and computational burden, as well as to the impact of specific techniques such as piecewise affine linearization and rolling horizon control.

4.1. Computational performance and scalability of optimization models

MILP algorithms are generally expected to provide a high accuracy level for the models analyzed in this work, due to their being based on exact mathematical optimizations. These algorithms can ensure an optimal or nearly-optimal solution within a specific tolerance (MIP Gap), particularly for linear and piecewise linear problems [67]. However, as the size and complexity of a problem increase, MILP models can become computationally demanding and, in some cases, impractical. In this study, for example, the MILP_NL and MILP_C models had to face

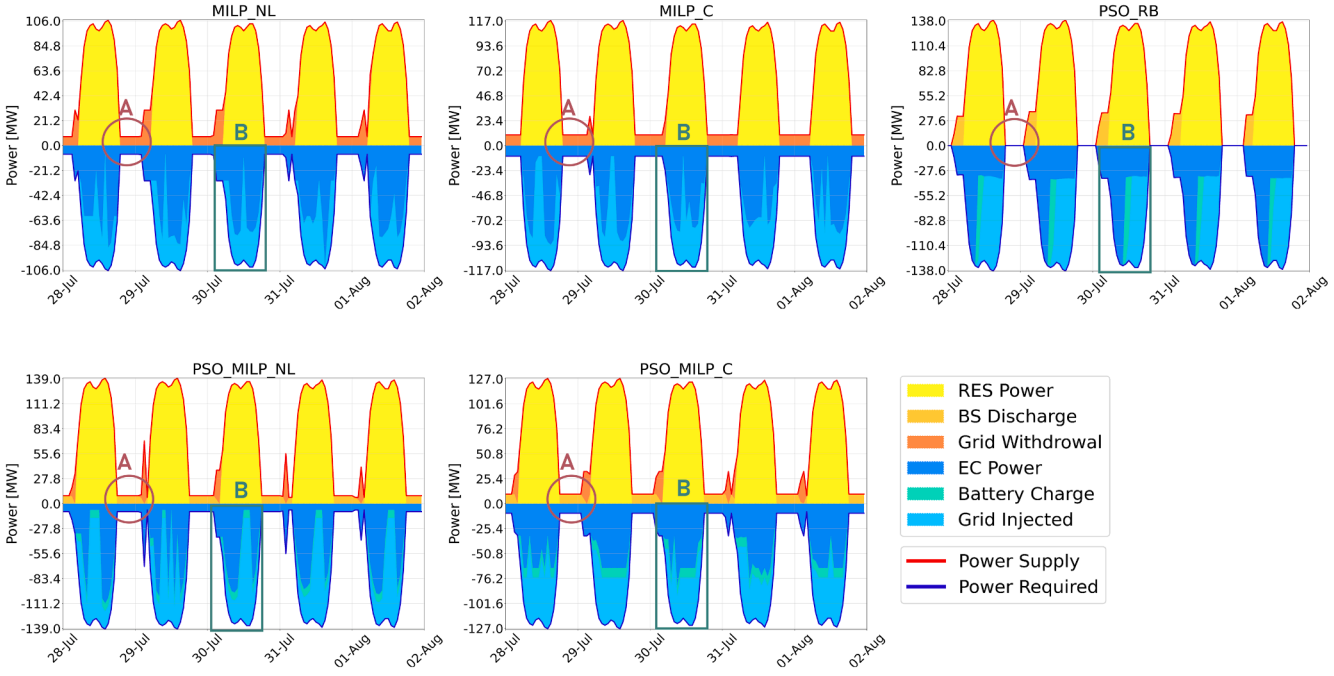

Fig. 11. Electric balance of the different models.

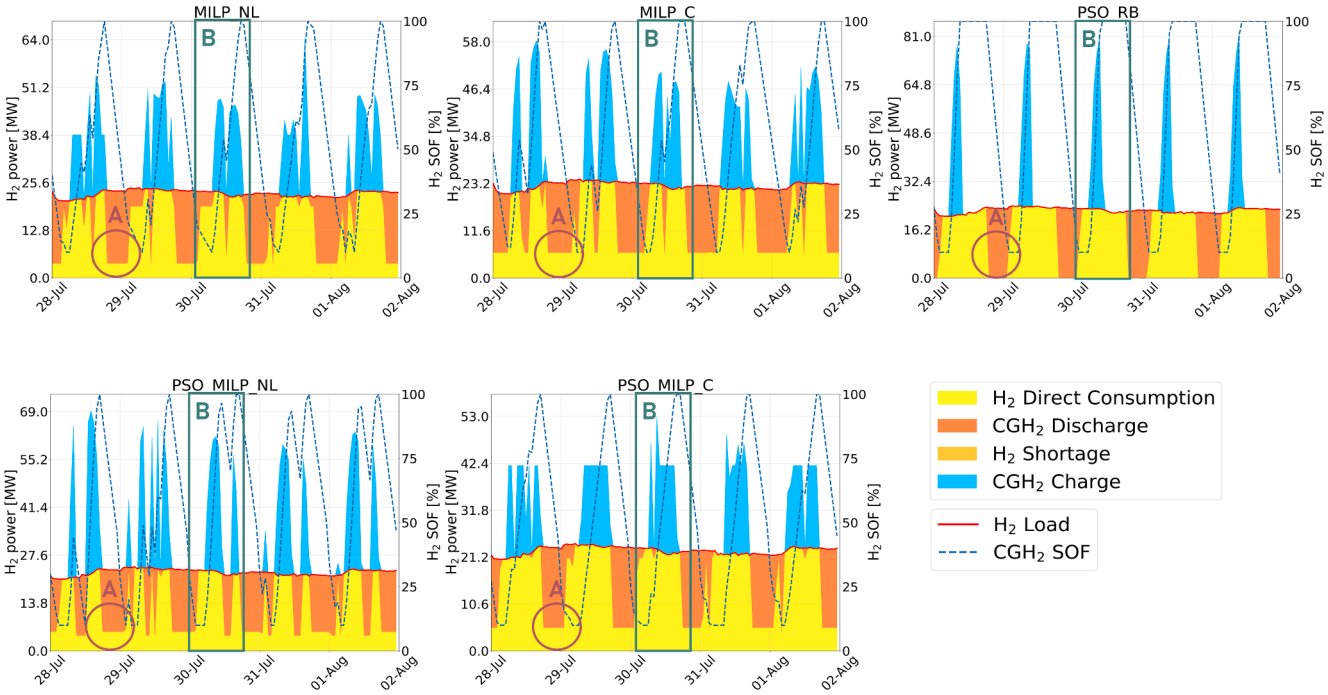

Fig. 12. Hydrogen balance of the different models.

significant computational challenges, and this led to suboptimal results, even after 48 h of computation. This computational burden in part arises because MILP requires a simultaneous optimization of design and scheduling over the entire time horizon, which leads to a large number of variables and constraints. Additionally, the need to piecewise-linearize the efficiency of the electrolyzer and account for battery degradation adds further complexity [68].

This scalability issue was particularly evident in the MILP_NL and MILP_C models analyzed in this study. Indeed, the computational time required to solve these problems was very high, and even after 48 h of computation, an optimal solution had still not been reached, thus resulting in suboptimal outcomes. The complexity of the computation was in particular increased by the need to track battery cycles and to compute degradation. For example, in the cases with constant efficiency and no degradation, the model achieved an MIPGap of less than 1 % within 30 s. However, when linear degradation was introduced, the model only achieved an MIPGap of 30 % after 48 h of computation. Additionally, the MILP_NL and the MILP_C models both had to face the limitation of not accounting for the depth of discharge of the battery in the degradation calculations. This simplification was necessary to avoid introducing non-linearities, which means that both sizing and scheduling were optimized under the assumption that the battery degradation only depended on the number of cycles and not on the state of charge.

Compared to non-linear formulations (e.g., MINLP), the adoption of piecewise affine linearization significantly improves the computational tractability of the MILP framework by enabling the representation of complex system behaviours within a linear structure. However, this inherently introduces an approximation of non-linear dynamics, leading to a trade-off between model fidelity and optimization feasibility that must be carefully considered. In this study, the PWA functions were designed to balance accuracy and computational efficiency, as supported by the low RMSE and high R^2 values reported in Section 2.2.1. Nevertheless, a full validation against high-fidelity non-linear models was not conducted, as such simulations would substantially increase the computational burden and fall beyond the scope of this work. Future studies could incorporate a direct comparison between MILP-PWA and MINLP formulations to quantify the impact of such approximations on system behaviour and economic outcomes. This direction is supported by previous findings – for example, Grimaldi et al. [61] showed that MILP-based simplifications yielded results with limited deviation from full non-linear formulations, while reducing computation times by more than an order of magnitude.

The model was adapted to a MILP, combined with a PSO framework with rolling horizon optimization, to mitigate this issue and reduce the computational time. In this way, the scheduling problem was broken down into smaller, more manageable, sub-problems over shorter time intervals. By optimizing these sub-problems sequentially, the rolling horizon approach was able to significantly reduce the computational burden, thus making the problem more manageable, although it still provided high-quality results. The PSO_MILP_NL and PSO_MILP_C models achieved a MIPGap of 1 % after 35 and 27 h, respectively. The PSO_RB model instead managed to optimize the design variables by relying on predefined rules for the energy management strategy, and it required only 1.5 h to converge on the optimal solution. A summary of computation time, convergence metrics, and PSO iteration settings is reported in Table S.4of the Supplementary Material.

These results may appear to contradict the conventional view that MILP is computationally more efficient than metaheuristic algorithms. However, such a view holds primarily for strictly linear or moderately sized problems. In this study, the need to approximate nonlinear behaviors (e.g., electrolyzer efficiency, battery degradation) with piecewise functions, coupled with the simultaneous optimization of design and scheduling over long horizons, leads to MILP formulations with a high number of variables and constraints. As a result, the computational cost of MILP becomes comparable to, or even exceeds, that of heuristic methods, particularly when solution accuracy (e.g., low MIP gap) is required. Conversely, metaheuristics like PSO, while inherently approximate and reliant on population-based search, can more flexibly accommodate nonlinearities and discontinuities in the system model, potentially yielding solutions that are closer to real-world operational feasibility. This reinforces the notion that algorithmic efficiency must be assessed in light of the actual problem formulation, not in abstract terms.

A more detailed analysis of the convergence behavior of the PSO-based models is provided in Fig. S.5 and Fig. S.6 of the Supplementary Material. These figures illustrate how the LCOH evolves throughout the

optimization process. In particular, Fig. S.6 shows that all PSO models exhibit a clear and stable convergence trend within the specified number of iterations, confirming the reliability of the solution. Indeed, the number of particles (30) and iterations (50) were selected to ensure a balance between convergence and computational effort. As expected, the PSO_RB model converges faster due to its reduced problem dimensionality, while the hybrid PSO-MILP models require more iterations to refine the solution in a higher-dimensional, constrained design space.

It is worth noting that, although PSO was selected for its demonstrated robustness and performance, a wider comparison across multiple metaheuristic algorithms – including Grey Wolf Optimization, Harmony Search, Constrained PSO, Flower Pollination Algorithm [69–71], and emerging strategies such as the Mayfly or Arctic Puffin optimization [72,73] – could provide further insights into trade-offs between convergence, scalability, and model interpretability. In this context, incorporating comparative experiments with additional advanced algorithms may further extend the research scope and strengthen the generalization of the conclusions. Future studies may explore such algorithms to expand on the optimization landscape presented in this work and validate the performance robustness of the proposed hybrid strategies.

4.2. Cost-emission trade-offs, operational strategies, and environmental performance

A key trade-off highlighted by the aforementioned results is the balance between minimizing the levelized cost of hydrogen and reducing greenhouse gas emissions. To further explore this balance, a Pareto front was constructed based on all solutions generated during the PSO_RB optimization process. As illustrated in Fig. S7 of the Supplementary Material, the resulting front delineates a clear non-linear relationship between the levelized cost of hydrogen and CO_2 emissions. Solutions located at the lower end of the emissions spectrum are associated with markedly higher production costs, while those achieving minimal LCOH values tend to exhibit significantly greater environmental impacts. This distribution underscores the absence of a single optimal solution, instead revealing a continuum of Pareto-efficient outcomes that enable flexible prioritization between competing objectives. The selected PSO_RB configuration is located on this front, thereby confirming its status as a cost-effective and environmentally responsible compromise within the feasible design space.

In order to meet the EU's renewable hydrogen threshold, the GHG emission intensity must be below 3 kg_{CO2} per kg of hydrogen produced [54]. Only the PSO_RB model satisfied this standard, with an emission intensity of 2.38 kg_{CO2}/kg_{H2}, while the other models approached but did not meet the threshold. PSO_MILP_NL and PSO_MILP_C showed emission intensities of between 3.2 and 3.3 kg_{CO2}/kg_{H2}, whereas MILP_C and MILP_NL reached even higher values of 3.4 and 4.1 kg_{CO2}/kg_{H2}, respectively. These findings suggest that, although the models attempted to balance cost and emissions, they did not always achieve the required environmental standard levels, thereby highlighting the necessity of trade-offs to achieve the pre-determined LCOH and CO_2 emission levels.

The CO_2 intensity of electricity imported from the grid was assumed to be constant at 250 g_{CO2}/kWh, reflecting the average European grid value [54]. While real-world grid emission intensity is time-varying and dependent on the hourly mix of generation technologies, the use of a static emission factor was motivated by the need to maintain computational tractability and methodological consistency across models. Incorporating dynamic marginal emission profiles would have required additional data processing and significantly increased model complexity and solver time, particularly for MILP-based models already characterized by long computation durations. Moreover, given the objective of comparing different optimization strategies under consistent boundary conditions, a fixed emission factor ensured a fair and controlled assessment. Nevertheless, future work could explore the impact of time-varying CO_2 intensities on the environmental performance of hybrid systems by leveraging country-specific marginal emission datasets or real-time grid mix data.

The LCOH results ranged from 10.1 to 10.7 €/kg for the MILP_NL and MILP_C models, from 9.7 to 9.2 €/kg for the PSO_MILP_NL and PSO_MILP_C models and reached 11.6 €/kg for the PSO_RB model. These values are broadly aligned with findings in the pertinent literature but reflect certain differences, due to their underlying assumptions. Stolte et al. [54] reported LCOH values that ranged between 2.5 and 9 €/kg, with corresponding emission intensities ranging from 14.2 kg_{CO2}/kg_{H2}, for high electricity prices, to as low as 0.1 kg_{CO2}/kg_{H2}, for optimal conditions with low electricity prices and high renewable penetration. The lower LCOH values may partially have resulted from their inclusion of wind power, which typically features a higher capacity factor than solar PV, thereby reducing the overall cost of the electricity used for hydrogen production.

Similarly, Abomazid et al. [74] analyzed the cost of hydrogen of a system that integrates BESS and solar PV and reported LCOH values of between 5.39 and 8.74 €/kg, which were slightly lower than the results of this study. This discrepancy can be attributed to their assumption of a battery cost of 100 $/kWh, which was significantly lower than the cost considered in this study. Furthermore, neither of the aforementioned authors accounted for the impact of battery degradation on the performance and costs of the system, which is explicitly modeled in this work. The inclusion of battery degradation introduced additional operational constraints and increased the lifecycle costs, thereby resulting in higher LCOH values.

It should be recalled that the outcomes of this study (like any other study of this kind) are inherently sensitive to external market conditions, such as the electricity purchase and sale price ratios, as well as storage costs. Changes in these market dynamics could lead to different optimization strategies and potentially alter the results observed herein. Moreover, including revenues from electricity sales to the grid in the LCOH objective function, could incentivize the oversizing of the PV capacity to maximize grid sales, as previously highlighted in the literature [54,62]. However, in this work, this type of oversizing was mitigated by several key factors. These include the constraints imposed on the maximum PV capacity, the disparity between the purchase and sale prices of electricity, and the degradation and inefficiency costs associated with energy storage systems. Collectively, these constraints ensured that the optimization process remained focused on hydrogen production and efficient storage management, rather than overly prioritizing grid sales.

The power limit of 200 MW adopted for the PV system reflects practical considerations related to the size of the installation. A 200 MW PV plant would occupy an area of approximately 6–8 km^2, assuming a standard land-use efficiency of around 25–35 MW per km^2 for utility-scale solar farms, depending on the efficiency and layout of the panels [75]. This capacity is aligned with the typical range adopted for utility-scale plants, which are often designed to deliver power over the 100–500 MW range, thereby ensuring feasibility while accommodating land constraints [76].

Similarly, the energy storage capacities were capped at 200 MWh because of space-related considerations. This value corresponds to a volume of approximately 2,000–2,500 m^3 for hydrogen storage at 30 bar, depending on the design and storage capacity of the tank. A value of 200 MWh represents a substantial footprint for BESS, given the energy density of modern lithium-ion batteries, which typically have an estimated physical volume of 1000 m^3 for the required capacity (volumetric energy density of 200 kWh/m^3 [77]). These limitations ensure the

feasibility of their integration in industrial-scale applications, while remaining consistent with the typical operational and economic constraints of large-scale renewable energy systems. Moreover, these sizes are aligned with the benchmarks for utility-scale technologies, as reported by NREL (National Renewable Energy Laboratory) in their 2024 Annual Technology Baseline Database [78], which provides standardized references for the modeling and design of energy systems.

Although the considered optimizer theoretically has the flexibility to draw energy from any source – PV, BESS or the grid – it exclusively utilizes PV energy for resale to the grid. This outcome is primarily driven by economic factors: the selling price to the grid is lower than the cost of purchasing electricity, thus any grid-to-grid interaction is effectively excluded from consideration. Additionally, the costs associated with battery degradation, which are compounded by conversion inefficiencies during the charging and discharging cycles, make it economically unfeasible to resell stored energy. Indeed, the marginal financial benefit of selling battery-stored power is outweighed by the associated losses. As a result, the optimizer prioritizes more cost-effective strategies, such as that of directly using or selling surplus PV energy, and it avoids scenarios in which stored energy is discharged for sale on the grid.

Another important aspect of optimization is that the battery utilization rates underscore the trade-offs between grid reliance, battery size, and degradation. The rule-based PSO_RB model exhibited higher battery utilization, that is, around 173 cycles per year, thus reflecting its minimal dependence on grid imports and its attempt to maximize the use of the available stored energy. Conversely, the MILP_NL model, with only 16 battery cycles per year, relied more heavily on grid imports, which resulted in a lower battery usage and, therefore, underutilization of the battery investment. The PSO_MILP_NL and PSO_MILP_C models achieved more balanced results, with battery cycles of 140 and 162 per year, respectively. These findings are aligned with the existing literature on energy arbitrage. Grimaldi et al. [61], for instance, suggested cycle frequencies that ranged from 155 to 450 per year, depending on the degradation costs. Similarly, Cetinkaya et al. [79] calculated battery cycle frequencies of between 325 and 390 per year, with an aging of 1.08–1.2 %.

Given a battery lifespan of 20 years and 7000 cycles, the optimal cycle frequency would be around 350 cycles per year. Utilization rates below this threshold would suggest that the full potential of the battery investment is not being exploited. Indeed, investing in an expensive battery, but underutilizing it, could lead to suboptimal returns, especially since BESS costs are expected to decrease in the future.

While the present analysis is based on deterministic inputs for load, PV generation, electricity prices, and hydrogen demand, future work could incorporate uncertainty modeling through stochastic optimization or scenario-based approaches. This would support a more robust assessment of the trade-offs between cost, emissions, and reliability, thereby improving the resilience of the selected optimization strategies.

4.3. Implementation costs and practical feasibility

Finally, transitioning from a rule-based control system, which is typically implemented on a Programmable Logic Controller (PLC), to an advanced optimization-based approach that utilizes mixed-integer linear programming with a rolling horizon, presents a significant shift in both capital and operational expenditures. Although PLC-based systems are relatively cheap and suitable for routine, low-level control tasks, a MILP-based approach requires considerably more computational resources and incurs higher initial and operational costs.

In general, a PLC designed for industrial applications costs between €500 and €5,000, depending on its processing power, input/output capabilities, and communication features. These controllers are energy-efficient and are built for rugged environments, thus making them highly reliable and requiring limited maintenance. Operating such a system is relatively cheap, as PLCs are optimized for continuous operation and have minimal computational overheads.

On the other hand, a system designed to handle MILP-based optimization, particularly one that is capable of performing real-time or near-real-time computations, requires a significantly more powerful computational setup. The hardware costs for a basic workstation capable of handling moderate MILP problems can start at around €1,000 and may reach up to €10,000 for high-performance workstations with advanced multi-core CPUs, extensive RAM, and fast storage options. More powerful setups, such as dedicated servers or high-performance computing systems, may be necessary for applications that involve large-scale MILP problems or time-sensitive optimization. Such systems can range from €10,000 to €30,000, depending on the specific processing and memory requirements.

Additionally, MILP-based optimization requires specialized software and solver licenses, thereby adding to the overall cost. Industrial-grade MILP solvers, such as Gurobi, CPLEX, or MOSEK, often have annual licensing fees that can range from €5,000 to €20,000, depending on the computational scale and the number of used cores. Further costs can arise if custom software development or integration with demand forecasting models is required, especially when accurate demand and PV production predictions are essential for system optimization. Incorporating forecasting introduces additional costs for data acquisition, sensor networks, and machine learning models, which further increases both the computational demands and the licensing expenses.

The overall costs of a PLC-based, RB system versus an optimized, MILP-PSO system are summarized in Table 4. The table provides a cost comparison that includes both hardware and software expenditures.

Apart from the initial setup and licensing costs, MILP-PSO systems also have higher operational costs, due to their increased energy consumption. Although PLCs typically consume around 10–50 W, the high-performance computing systems that are required for MILP can consume hundreds of watts, thereby impacting the long-term energy expenses. Moreover, MILP optimization is inherently more complex, and it requires regular updates, predictive data inputs, and maintenance of both the hardware and software components, all of which adds further costs.

Although the MILP-based strategies employed in this study rely on full-year simulations with perfect foresight, such formulations are primarily intended as reference benchmarks to evaluate the theoretical performance of different optimization paradigms. In real-world applications, these strategies are impractical for real-time implementation due to their substantial computational demands and the requirement for complete a priori knowledge of system inputs. In contrast, heuristic methods or hybrid MILP approaches embedded within rolling horizon frameworks are more suitable for deployment, as they can incorporate updated forecasts and respond adaptively to time-varying system conditions under uncertainty.

Table 4
Comparison of the overall costs of plc-based, rule-based models and milp-pso optimized systems.

System	Estimated Hardware Cost [€]	Estimated Software/ License Cost [€]	Total Estimated Cost [€]
PLC (Rule-Based)	500–5,000	None or Low	500–5,000
MILP Workstation	1,000–10,000	5,000–20,000	6,000–30,000
High-End MILP Server	10,000–30,000	10,000–30,000	20,000–60,000

5. Conclusions

This study has compared multiple optimization strategies – MILP, PSO, and hybrid approaches – for the design and operational management of hybrid hydrogen systems, with particular attention to algorithms performance under increasing model complexity, including nonlinear efficiency and degradation effects.. The results have revealed substantial differences in the economic and environmental performances of the systems, depending on the chosen optimization strategy.

Beyond the comparative analysis, this work introduces several methodological innovations, including the use of piecewise affine linearization for electrolyzer efficiency and battery degradation in a sizing context, the extension of rolling horizon control to hybrid battery-hydrogen storage systems under dynamic pricing, and a structured evaluation of trade-offs between cost, emissions, and computational burden.

The PSO-based model with a rule-based energy management strategy (PSO_RB) demonstrated the best environmental performance, as it achieved the lowest CO_2 emissions. Although this approach led to an 8–26 % higher levelized cost of hydrogen, compared to the other models, it proved effective in reducing grid dependence and minimizing emissions. This trade-off highlights the importance of a comprehensive optimization approach that balances costs and environmental impacts. On the other hand, the MILP-based models (MILP_NL and MILP_C) were more cost-efficient, with lower LCOH values, but resulted in higher CO_2 emissions and a greater reliance on the grid.

The hybrid PSO-MILP models (PSO_MILP_NL and PSO_MILP_C) presented balanced solutions, as they reduced both grid imports and CO_2 emissions, while maintaining competitive LCOH values. These models, which benefited from the integration of rolling horizon optimization, improved the responsiveness to dynamic energy needs, thereby optimizing the balance between energy production, storage, and consumption.

Energy management strategies play a critical role in reducing grid dependence. The PSO_RB model effectively maximized the use of renewable energy sources (such as PV) and stored energy (batteries and hydrogen), thereby minimizing imports from the grid. The MILP models instead were more reliant on grid power, which affected their overall sustainability. Additionally, the PSO_RB model achieved the highest electrolyzer efficiency. Moreover, it operated closer to its nominal power levels and optimized renewable energy utilization. Hydrogen storage utilization was also found to be the most efficient for the PSO_RB model, which prioritized maintaining a full hydrogen capacity during PV production. This allowed the model to meet the energy demands during non-solar hours, without the need for grid imports, thus illustrating the importance of optimizing both battery and hydrogen storage to obtain the maximum efficiency of the system and a reduced LCOH.

These findings emphasize the need for a balancing of both the operational costs and carbon emissions when optimizing hybrid hydrogen systems. A hybrid approach that combines the strengths of MILP and PSO, along with advanced energy management strategies, appears to be the most promising solution for large-scale, hydrogen-production systems.

Further research could explore integrating non-linear functions, such as electrolyzer degradation and component investment cost functions on the basis of size, to improve the accuracy of the models. However, this would significantly increase the computational time, particularly for MILP models, due to the need for linearizing non-linear curves, which would add complexity to the optimization process and only provide marginal improvements to the results. Additionally, longer time horizons could be considered to assess the performance of long-term, energy-storage systems, although this would drastically increase the computational times, potentially making such analyses impractical for large-scale systems.

Overall, this analysis demonstrates that model formulation and algorithmic strategy are deeply intertwined: the choice of optimization approach must be aligned not only with the design objectives (cost, emissions, reliability), but also with the level of model fidelity appropriate for the application context. While MILP-based strategies offer potential long-term cost savings in terms of LCOH, their performance is strongly affected by the complexity of the model. Contrary to conventional expectations, MILP formulations in this study resulted in longer computational times than heuristic approaches due to the high dimensionality and the need to approximate nonlinear behaviors. This confirms that algorithmic efficiency cannot be assessed independently of model structure and fidelity.

CRediT authorship contribution statement

Elena Rozzi: Writing – original draft, Visualization, Software, Methodology, Investigation, Formal analysis, Conceptualization. **Alberto Grimaldi:** Writing – review & editing, Methodology, Conceptualization. **Francesco D. Minuto:** Writing – review & editing, Supervision, Methodology, Conceptualization. **Andrea Lanzini:** Writing – review & editing, Supervision, Methodology, Conceptualization.

Declaration of competing interest

The authors declare that they have no known competing financial interests or personal relationships that could have appeared to influence the work reported in this paper.

Acknowledgements

This study was carried out as part of the National Recovery and Resilience Plan (PNRR) and received funding from the Italian Ministry of the Environment and Energy Security, for the “Novel Materials for Hydrogen storage (NoMaH)” project, ID RSH2A_000035, CUP: F27G22000180006.

This manuscript only reflects the authors’ views and opinions, and neither the European Union nor the European Commission can be considered responsible for them.

Appendix A. Comparative overview of MILP-Based and metaheuristic optimization approaches for hybrid energy storage systems

Table A1
Comparative summary of MILP-based and metaheuristic optimization strategies for hybrid storage systems, highlighting linearization techniques, application scope, and integration of hydrogen technologies.

Ref.	Storage Type	Optimization Algorithm	Purpose	Rolling Horizon	Non-linearities	Focus	Notes
[22]	H_2 + BESS	Metaheuristics	Sizing	No	No	Comprehensive review	Environmental and socio-political parameters
[23]	H_2 + BESS	PSO, ABC, BBO, GA, HS, IWO, SCE, TBLO	Sizing	No	No	Algorithm comparison	PSO outperforms on convergence and cost
[80]	H_2 + BESS	ABC, CS, BB-BC, IC	Sizing	No	No	Hybrid storage comparison	Solar/wind + BESS more cost-effective
[24]	H_2 + SC	PSO, MFO, GA, DA, GIA, SSA, ALO, GWO	Sizing	No	No	Microgrid cost minimization	MFO most stable, PSO fastest
[25]	H_2 + BESS	MFO, GWO, MVO. AVOA	Sizing	No	No	Thermal plant replacement	Hybrid config reduces sizing needs
[26]	H_2 + BESS	PSO	Sizing	No	No	Production cost minimization	Waste fermentation/natural gas reforming
[81]	H_2 + BESS + SC	Hybrid JSPSOBAT (Jellyfish, PSO, BAT)	Scheduling	No	No	EMS strategy testing	Multi-algorithm hybridization
[17]	H_2 + BESS	MILP	Scheduling	No	No	Cost minimization	Linear battery degradation, H_2 prioritization
[25]	H_2 + BESS + Thermal	MILP	Scheduling	No	No	Emission and cost reduction	Focus on hybrid multi-energy microgrid
[21]	H_2 + BESS	MILP	Scheduling	No	No	Cost/emissions trade-off	PEM/SOEC comparison
[11]	H_2 + BESS	MILP	Scheduling	Yes	No	Forecast-based operation	Uses extra-day forecast info
[42]	H_2 + BESS	MILP	Scheduling	Yes	PWA	Efficiency impact	Scheduling shifts to higher efficiency
[31]	BESS	MILP	Scheduling	Yes	No	Microgrid scheduling	Confidence-weighted forecasts
[35]	BESS	MILP	Scheduling	Yes	No	Multi-objective control	Economic dispatch, BESS costs, peak shaving
[36]	BESS	MILP	Scheduling	Yes	No	BESS control in smart grid	Two-stage method for RES self-consumption
[32]	BESS	MILP	Scheduling	Yes	QP	Smart home energy optimization	Real-time pricing; dynamic load management
[33]	BESS	MILP	Scheduling	Yes	No	Interval length sensitivity	SOC preservation vs early depletion
[30]	BESS	MILP	Scheduling	Yes	Parametric	Uncertainty-aware EMS	EV-integrated microgrid
[43]	H_2 + BESS	MILP	Scheduling	Yes	PWA	Electrolyzer/fuel cell modeling	Includes temperature dynamics in PWA
[44]	BESS	MILP	Scheduling	Yes	PWA	Battery degradation	PWA of damage per cycle vs DOD
[45]	BESS	MILP	Scheduling	No	PWA	Degradation and conversion loss	2D PWA for SOC and power
[38]	BESS	MILP	Scheduling	Yes	PWA	Cycle-counting integration	Real-time cycle counting for degradation
[39]	BESS	MILP	Scheduling	Yes	PWA	Cycle counting	Convexity-based real-time RCA
[40]	BESS	MILP	Scheduling	Yes	No	Cycle counting	RCA vs conventional cycle counting
[13]	H_2 + BESS	MILP + Stochastic	Scheduling	No	No	Uncertainty-aware EMS	Multiple sources and demand response
[14]	H_2 + BESS	MILP + Stochastic	Scheduling	No	No	Renewables uncertainty	MILP with stochastic model (Monte Carlo)
[15]	H_2 + BESS + Heat	MILP + Stochastic	Scheduling	No	No	Demand response integration	Two-stage risk-constrained model
[27]	BESS + Pump hydro	MILP + PSO	Scheduling	No	PWA	Hybrid optimization for microgrid	MILP for initialization, PSO for refinement
[82]	BESS + Heat	MILP + PSO	Scheduling	Yes	PWA	Multi-scale operation planning	MILP for plan, PSO for daily adjustment
[83]	BESS	MILP + PSO	Scheduling	Yes	PWA	Hierarchical scheduling	MILP for internal, PSO for inter-microgrid
[84]	H_2 + BESS	MILP + PSO	Scheduling	No	No	Integrated energy systems	Scheduling with hybrid model
[85]	H_2 + BESS	MISOCP, MILP	Sizing + Scheduling	No	MISOCP	Techno-economic analysis	MISOCP vs MILP using nonlinear efficiencies
[18]	H_2 + BESS	MILP	Sizing + Scheduling	No	No	Two-step optimization	Min system costs and max energy stored
[19]	H_2 + BESS	MILP	Sizing + Scheduling	No	KKT	Multi-microgrid co-optimization	Bi-layer model optimizing profits and costs
[10]	H_2 + BESS	MILP	Sizing + Scheduling	No	Linearized MINLP	Electric and thermal load	Binary-continuous product linearization
[16]	H_2 + BESS	MILP	Sizing + Scheduling	No	PWA	Real-time pricing and planning	Seawater electrolysis substitutes BESS

(*continued on next page*)

Table A1 (*continued*)

Ref.	Storage Type	Optimization Algorithm	Purpose	Rolling Horizon	Non-linearities	Focus	Notes
[41]	H_2 + BESS	MILP	Sizing + Scheduling	No	PWA	Electrolyzer/fuel cell efficiency	PWA for efficiency and investment cost
[12]	H_2 + BESS	MILP + GA	Sizing + Scheduling	Yes	No	EMS strategy comparison	Short-term forecasting uncertainties
[34]	H_2 + BESS	MILP + GA	Sizing + Scheduling	Yes	No	Off-grid system optimization	GA for sizing, rolling horizon-MILP for EMS
[86]	–	MILP vs PSO	Sizing + Scheduling	No	LinDistFlow	Comparative performance	MILP (GAMS) vs PSO (pypower)
[87]	H_2 + BESS	MILP + PSO	Sizing + Scheduling	Yes	No	Energy management	MILP/LP for scheduling; PSO for BESS sizing
[88]	–	MILP + PSO	Sizing + Scheduling	No	No	Multi-year optimization	PSO for capacity, MILP for operation
[28]	H_2 + BESS	MILP + PSO	Sizing + Scheduling	Yes	No	Bi-level co-optimization	PSO for sizing, MILP for scheduling
[29]	H_2 + BESS	MILP + PSO	Sizing + Scheduling	Yes	PWA	EMS strategy comparison	Rolling horizon vs single-layer MILP
This study	H2 + BESS	MILP + PSO	Sizing + Scheduling	Yes	PWA	Optimization algorithms comparison	Rolling horizon and PWA for BESS degradation and electrolyser efficiency

MISOCP: Mixed Integer Second Order Conic Programming
AVOA: African Vulture Optimization Algorithm
ABC: Artificial Bee Colony
BBO: Biogeography-Based Optimization
HS: Harmony Search
SCE: Shuffled Complex Evolution
TLBO: Teaching–Learning Based Optimization
CS: Cuckoo Search
BB-BC: Big Bang-Big Crunch
IC: Imperialist Competitive
DA: Dragonfly Algorithm
SSA: Salp Swarm Algorithm
ALO: Ant Lion Optimizer
GWO: Grey Wolf Optimizer
GOA: Grasshopper Optimization Algorithm
IWO: Invasive Weed Optimization
MVO: Multi-Verse Optimizer
KKT: Karush-Kuhn-Tucker
SC: Supercapacitor
QP: Quadratic Programming

Appendix B. — Hyperparameter calibration for PSO Algorithm

The selection of PSO hyperparameters was based on a multi-phase calibration process aimed at balancing solution quality and computational cost. The procedure, applied to the PSO_RB model due to its reduced simulation time compared to PSO_MILP, began with a grid search over constant values for the cognitive coefficient (c_1), social coefficient (c_2), and inertia weight (w), followed by the evaluation of time-dependent decay strategies. Linear decay, decreasing c_1 and w while increasing c_2 over time, consistently yielded better convergence behavior and was therefore retained. Subsequent tests fine-tuned the decay profiles and assessed the impact of swarm size and iteration count, confirming that larger configurations provided only marginal improvements at the cost of significantly increased runtime. Finally, velocity- and boundary-handling strategies were compared, with "unmodified" and "periodic" offering the most stable and efficient results. The tested ranges and selected values are reported in Table B1, and detailed results are available in the supplementary Excel file.

Table B1
PSO parameter selection via grid search: tested ranges and optimal parameter settings.

Parameter category	Parameter	Values tested	Optimal selected
Acceleration coefficients and inertia weight	Cognitive coefficient	Constant values between 0.5 and 2.5, and decay schemes (linear, non-linear, exponential) in the same range	Linear decay: from 2.5 to 0.5
	Social coefficient	Constant values between 0.5 and 2.5, and decay schemes (linear, non-linear, exponential) in the same range	Linear increase: from 0.5 to 2.5
	Inertia weight	Constant values between 0.1 and 1, and decay schemes (linear, non-linear, exponential) in the same range	Linear decay: from 1 to 0.1
Number of particles and iterations	Number of particles	30, 50, 100, 150	30
	Number of iterations	50, 100, 150, 200, 300	50
Velocity handling strategy	Velocity handling method	unmodified, adjust, invert, zero	unmodified
Boundary handling strategy	Boundary handling method	periodic, nearest, random, shrink, reflective, intermediate	periodic

Appendix B. Supplementary material

Supplementary data to this article can be found online at https://doi.org/10.1016/j.enconman.2025.120306.

Data availability

Data will be made available on request.

References

[1] IEA, Tracking Clean Energy Progress 2023 - Hydrogen, IEA (2023). https://www.iea.org/energy-system/low-emission-fuels/hydrogen (accessed August 26, 2024).
[2] IEA, Tracking Clean Energy Progress 2023 - Industry, IEA (2023). https://www.iea.org/energy-system/industry (accessed August 26, 2024).
[3] IEA, Global hydrogen review 2023, IEA, Paris, 2023. https://www.iea.org/reports/global-hydrogen-review-2023.
[4] IEA, Net Zero Emissions Guide - Hydrogen, IEA, Paris, 2023. https://www.iea.org/reports/hydrogen-2156 (accessed August 26, 2024).
[5] IEA, Tracking Clean Energy Progress 2023 – Analysis, IEA, Paris, 2023. https://www.iea.org/reports/tracking-clean-energy-progress-2023 (accessed August 26, 2024).
[6] Yang Y, Wu Z, Yao J, Guo T, Yang F, Zhang Z, et al. An overview of application-oriented multifunctional large-scale stationary battery and hydrogen hybrid energy storage system. Energy Rev 2024;3:100068. https://doi.org/10.1016/j.enrev.2024.100068.
[7] Møller KT, Jensen TR, Akiba E, Li H. Hydrogen - a sustainable energy carrier. Prog Nat Sci: Mater Int 2017;27:34–40. https://doi.org/10.1016/j.pnsc.2016.12.014.
[8] Gao Q, Yang Z, Li W. Prospect on operations research for mixed-integer linear programming problems in power systems. Trans China Electrotech Soc 2024;39:3291–307. https://doi.org/10.19595/j.cnki.1000-6753.tces.230478.
[9] Bragin MA, Tucker EL. Surrogate "level-based" lagrangian relaxation for mixed-integer linear programming. Sci Rep 2022;12:22417. https://doi.org/10.1038/s41598-022-26264-1.
[10] Zhang Y, Hua QS, Sun L, Liu Q. Life Cycle optimization of renewable energy systems configuration with hybrid battery/hydrogen storage: a comparative study. J Storage Mater 2020;30:101470. https://doi.org/10.1016/j.est.2020.101470.
[11] Dai W, Chen J, Zhang Y, Lin D, Shi Y. Optimal day-ahead operation strategy of an electricity-hydrogen integrated energy system considering extra-day forecast information. IEEE Sustain Power Energy Conf (iSPEC) 2021;2021:863–70. https://doi.org/10.1109/iSPEC53008.2021.9735690.
[12] Xie Y, Ueda Y, Sugiyama M. Greedy energy management strategy and sizing method for a stand-alone microgrid with hydrogen storage. J Storage Mater 2021;44:103406. https://doi.org/10.1016/j.est.2021.103406.
[13] Eghbali N, Hakimi SM, Hasankhani A, Derakhshan G, Abdi B. Stochastic energy management for a renewable energy based microgrid considering battery, hydrogen storage, and demand response. Sustain Energy Grids Networks 2022;30:100652. https://doi.org/10.1016/j.segan.2022.100652.
[14] Son Y-G, Kim S-Y, Bae I-S. Optimal coordination of energy coupling system considering uncertainty of renewable energy sources. Energies 2024;17:931. https://doi.org/10.3390/en17040931.
[15] Nasir M, Rezaee Jordehi A, Tostado-Véliz M, Mansouri SA, Sanseverino ER, Marzband M. Two-stage stochastic-based scheduling of multi-energy microgrids with electric and hydrogen vehicles charging stations, considering transactions through pool market and bilateral contracts. Int J Hydrogen Energy 2023;48:23459–97. https://doi.org/10.1016/j.ijhydene.2023.03.003.
[16] Gamil MM, Sugimura M, Nakadomari A, Senjyu T, Howlader HOR, Takahashi H, et al. Optimal sizing of a real remote japanese microgrid with sea water electrolysis plant under time-based demand response programs. Energies 2020;13:3666. https://doi.org/10.3390/en13143666.
[17] Diabate M, Krishnamoorthy HS, Shi J. Optimal energy management of a hydrogen and battery-based energy storage system (ess) for future dc microgrids. In: 2023 IEEE International Conference on Power Electronics, Smart Grid, and Renewable Energy (PESGRE); 2023. p. 1–6. https://doi.org/10.1109/PESGRE58662.2023.10405233.
[18] Giovanniello MA, Wu X-Y. Hybrid lithium-ion battery and hydrogen energy storage systems for a wind-supplied microgrid. Appl Energy 2023;345:121311. https://doi.org/10.1016/j.apenergy.2023.121311.
[19] Deng H, Wang J, Shao Y, Zhou Y, Cao Y, Zhang X, et al. Optimization of configurations and scheduling of shared hybrid electric-hydrogen energy storages supporting to multi-microgrid system. J Storage Mater 2023;74:109420. https://doi.org/10.1016/j.est.2023.109420.
[20] Shi Z, Fan F, Tai N, Qing C, Meng Y, Guo R. An optimal operation strategy for integrated energy-logistics system in green port. IEEE/IAS Indust Commercial Power System Asia (I&CPS Asia) 2022;2022:1592–7. https://doi.org/10.1109/ICPSAsia55496.2022.9949685.
[21] Hassan A, Al-Awami AT, Muqbel AM, Fouad WA. Optimal day-ahead management of a hydrogen-based energy hub considering different electrolyzer technologies. IEEE Int Conf Energy Technol Future Grids (ETFG) 2023;2023:1–5. https://doi.org/10.1109/ETFG55873.2023.10407278.
[22] Eriksson ELV, MacA E. Gray, Optimization and integration of hybrid renewable energy hydrogen fuel cell energy systems – a critical review. Appl Energy 2017;202:348–64. https://doi.org/10.1016/j.apenergy.2017.03.132.
[23] Phan-Van L, Takano H, Nguyen Duc T. A comparison of different metaheuristic optimization algorithms on hydrogen storage-based microgrid sizing. Energy Rep 2023;9:542–9. https://doi.org/10.1016/j.egyr.2023.05.152.
[24] Mohseni S, Brent AC, Burmester D. A comparison of metaheuristics for the optimal capacity planning of an isolated, battery-less, hydrogen-based micro-grid. Appl Energy 2020;259:114224. https://doi.org/10.1016/j.apenergy.2019.114224.
[25] Amoussou I, Tanyi E, Fatma L, Agajie TF, Boulkaibet I, Khezami N, et al. The optimal design of a hybrid solar pv/wind/hydrogen/lithium battery for the replacement of a heavy fuel oil thermal power plant. Sustainability 2023;15:11510. https://doi.org/10.3390/su151511510.
[26] HassanzadehFard H, Tooryan F, Dargahi V, Jin S. A cost-efficient sizing of grid-tied hybrid renewable energy system with different types of demands. Sustain Cities Soc 2021;73:103080. https://doi.org/10.1016/j.scs.2021.103080.
[27] Kim R-K, Glick MB, Olson KR, Kim Y-S. MILP-PSO combined optimization algorithm for an islanded microgrid scheduling with detailed battery ESS efficiency model and policy considerations. Energies 2020;13:1898. https://doi.org/10.3390/en13081898.
[28] Han Y, Li L, Chen W, Hou Y, Zhang J. A bi-cyclic co-optimization method for sizing of electricity-hydrogen hybrid energy storage microgrid. Sustain Energy Fuels 2022;6:4048–61. https://doi.org/10.1039/D2SE00556E.
[29] Micangeli A, Fioriti D, Cherubini P, Duenas-Martinez P. Optimal design of isolated mini-grids with deterministic methods: matching predictive operating strategies with low computational requirements. Energies 2020;13:4214. https://doi.org/10.3390/en13164214.
[30] Erichsen G, Zimmermann T, Kather A. Effect of different interval lengths in a rolling horizon milp unit commitment with non-linear control model for a small energy system. Energies 2019;12:1003. https://doi.org/10.3390/en12061003.
[31] Gao H-C, Choi J-H, Yun S-Y, Lee H-J, Ahn S-J. Optimal scheduling and real-time control schemes of battery energy storage system for microgrids considering contract demand and forecast uncertainty. Energies 2018;11:1371. https://doi.org/10.3390/en11061371.
[32] Sanabria-Torres EA, Luna AC, Diaz NL, Andrade-Rengifo F. State-of-charge equalizations comparison in a multi-prosumer environment based on real-time energy management systems with iot-support. IEEE Appl Power Electr Conf Exposition (APEC) 2023;2023:614–9. https://doi.org/10.1109/APEC43580.2023.10131516.
[33] Wang H, Meng K, Dong ZY, Xu Z, Luo F, Wong KP. Efficient real-time residential energy management through MILP based rolling horizon optimization. IEEE Power & Energy Soc General Meeting 2015;2015:1–6. https://doi.org/10.1109/PESGM.2015.7285754.
[34] Rullo P, Braccia L, Luppi P, Zumoffen D, Feroldi D. Integration of sizing and energy management based on economic predictive control for standalone hybrid renewable energy systems. Renew Energy 2019;140:436–51. https://doi.org/10.1016/j.renene.2019.03.074.
[35] Malysz P, Sirouspour S, Emadi A. MILP-based rolling horizon control for microgrids with battery storage. In: IECON 2013–39th Annual Conference of the IEEE Industrial Electronics Society; 2013. p. 2099–104. https://doi.org/10.1109/IECON.2013.6699455.
[36] Elkazaz M, Sumner M, Pholboon S, Thomas D. Microgrid energy management using a two stage rolling horizon technique for controlling an energy storage system. In: 2018 7th International Conference on Renewable Energy Research and Applications (ICRERA); 2018. p. 324–9. https://doi.org/10.1109/ICRERA.2018.8566761.
[37] D'Ambrosio C, Lodi A, Martello S. Piecewise linear approximation of functions of two variables in MILP models. Oper Res Lett 2010;38:39–46. https://doi.org/10.1016/j.orl.2009.09.005.
[38] Wicke M, Bocklisch T. Hierarchical energy management of hybrid battery storage systems for pv capacity firming and spot market trading considering degradation costs. IEEE Access 2024;12:52669–86. https://doi.org/10.1109/ACCESS.2024.3387748.
[39] R. Nebuloni, L. Meraldi, L. Moretti, V. Ilea, C. Bovo, A. Berizzi, P. Raboni, A Real-Time Cycle Counting Method for Battery Degradation Calculation in MILP Models, in: 2023 IEEE International Conference on Environment and Electrical Engineering and 2023 IEEE Industrial and Commercial Power Systems Europe (EEEIC / I&CPS Europe), 2023: pp. 1–6. DOI: 10.1109/EEEIC/ICPSEurope57605.2023.10194776.
[40] Upadhya S, Wagner MJ. A dispatch optimization model for hybrid renewable and battery systems incorporating a battery degradation model. J Energy Res Technol 2021;144. https://doi.org/10.1115/1.4052983.
[41] Marocco P, Ferrero D, Martelli E, Santarelli M, Lanzini A. An MILP approach for the optimal design of renewable battery-hydrogen energy systems for off-grid insular communities. Energy Conver Manage 2021;245:114564. https://doi.org/10.1016/j.enconman.2021.114564.
[42] Neisen V, Baader FJ, Abel D. Supervisory model-based control using mixed integer optimization for stationary hybrid fuel cell systems*. IFAC-PapersOnLine 2018;51:320–5. https://doi.org/10.1016/j.ifacol.2018.11.403.

[43] Gabrielli P, Flamm B, Eichler A, Gazzani M, Lygeros J, Mazzotti M. Modeling for optimal operation of PEM fuel cells and electrolyzers. In: 2016 IEEE 16th International Conference on Environment and Electrical Engineering (EEEIC); 2016. p. 1–7. https://doi.org/10.1109/EEEIC.2016.7555707.
[44] Keske C, Srinivasan A, Sansavini G, Gabrielli P. Optimal economic and environmental arbitrage of grid-scale batteries with a degradation-aware model. Energy Convers Manage: X 2024;22:100554. https://doi.org/10.1016/j.ecmx.2024.100554.
[45] Peñaranda AF, Romero-Quete D, Cortés CA. Grid-scale battery energy storage for arbitrage purposes: a Colombian case. Batteries 2021;7:59. https://doi.org/10.3390/batteries7030059.
[46] Energy Transition Model, Hourly curves for gas - Data export, (2024). https://energytransitionmodel.com/scenario/data/data_export/hourly-curves-for-gas (accessed July 25, 2024).
[47] Neuwirth M, Fleiter T, Manz P, Hofmann R. The future potential hydrogen demand in energy-intensive industries - a site-specific approach applied to Germany. Energy Conver Manage 2022;252:115052. https://doi.org/10.1016/j.enconman.2021.115052.
[48] European Commission, JRC Photovoltaic Geographical Information System (PVGIS), (2024). https://re.jrc.ec.europa.eu/pvg_tools/ (accessed July 26, 2024).
[49] Gestore Mercati Energetici, Excel Historical Data, (2024). https://www.mercatoelettrico.org/It/download/DatiStorici.aspx (accessed July 26, 2024).
[50] ARERA, Prezzi dell'energia elettrica per usi industriali 2014 - 2021, (2021). https://www.arera.it/fileadmin/allegati/dati/ra21/eepcfr2.xlsx (accessed July 26, 2024).
[51] European Hydrogen Observatory, The European hydrogen market landscape, European Hydrogen Observatory, 2023. https://observatory.clean-hydrogen.europa.eu/sites/default/files/2023-11/Report%2001%20-%20November%202023%20-%20The%20European%20hydrogen%20market%20landscape.pdf#:~:text=URL%3A%20https%3A%2F%2Fobservatory.clean (accessed July 31, 2024).
[52] Al-Shamma'a AA, Alturki, FA, Farh HMH. Techno-economic assessment for energy transition from diesel-based to hybrid energy system-based off-grids in Saudi Arabia. Energy Transit 2020;4:31–43. https://doi.org/10.1007/s41825-020-00021-2.
[53] Khare V, Khare C, Nema S, Baredar P. Chapter 8 - Case study: Solar–wind hybrid renewable energy system. In: Khare V, Khare C, Nema S, Baredar P, editors. Decision Science and Operations Management of Solar Energy Systems. Academic Press; 2023. p. 273–322. https://doi.org/10.1016/B978-0-323-85761-1.00009-3.
[54] Stolte M, Minuto FD, Lanzini A. Optimizing green hydrogen production from wind and solar for hard-to-abate industrial sectors across multiple sites in Europe. Int J Hydrogen Energy 2024;79:1201–14. https://doi.org/10.1016/j.ijhydene.2024.07.106.
[55] Marler RT, Arora JS. The weighted sum method for multi-objective optimization: new insights. Struct Multidisc Optim 2010;41:853–62. https://doi.org/10.1007/s00158-009-0460-7.
[56] NREL, Annual Technology Baseline (ATB), (2023). https://atb.nrel.gov/ (accessed July 31, 2024).
[57] Rozzi E, Minuto FD, Lanzini A. Techno-economic dataset for hydrogen storage-based microgrids. Data Brief 2024;56:110795. https://doi.org/10.1016/j.dib.2024.110795.
[58] Badgett A, Brauch J, Thatte A, Rubin R, Skangos C, Wang X, et al. Updated manufactured cost analysis for proton exchange membrane water electrolyzers. NREL United States 2024. https://doi.org/10.2172/2311140.
[59] D. Peterson, J. Vickers, D. DeSantis, Hydrogen production cost from PEM electrolysis - 2019, DOE Hydrogen and Fuel Cells Program Record, 2020. https://www.hydrogen.energy.gov/docs/hydrogenprogramlibraries/pdfs/19009_h2_production_cost_pem_electrolysis_2019.pdf.
[60] Rozzi E, Minuto FD, Lanzini A. Dynamic modeling and thermal management of a power-to-power system with hydrogen storage in microporous adsorbent materials. J Storage Mater 2021;41:102953. https://doi.org/10.1016/j.est.2021.102953.
[61] Grimaldi A, Minuto FD, Brouwer J, Lanzini A. Profitability of energy arbitrage net profit for grid-scale battery energy storage considering dynamic efficiency and degradation using a linear, mixed-integer linear, and mixed-integer non-linear optimization approach. J Storage Mater 2024;95:112380. https://doi.org/10.1016/j.est.2024.112380.
[62] Marocco P, Gandiglio M, Santarelli M. Optimal design of PV-based grid-connected hydrogen production systems. J Clean Prod 2024;434:140007. https://doi.org/10.1016/j.jclepro.2023.140007.
[63] Godula-Jopek A. Hydrogen Production: by Electrolysis. Germany: John Wiley & Sons; 2015.
[64] Pyomo Documentation 6.7.3, (2024). https://pyomo.readthedocs.io/en/stable/index.html (accessed July 24, 2024).
[65] Gurobi Optimization - Documentation, Gurobi Optimization (2024). https://www.gurobi.com/documentation/ (accessed July 24, 2024).
[66] L. James V. Miranda, PySwarms: a research toolkit for Particle Swarm Optimization in Python, (2018). http://joss.theoj.org/papers/10.21105/joss.00433 (accessed August 19, 2024).
[67] Al Owaifeer M, Al-Muhaini M. MILP-based technique for smart self-healing grids. IET Generat Transmission Distribution 2018;12:2307–16. https://doi.org/10.1049/iet-gtd.2017.1844.
[68] Urbanucci L. Limits and potentials of mixed Integer Linear programming methods for optimization of polygeneration energy systems. Energy Procedia 2018;148:1199–205. https://doi.org/10.1016/j.egypro.2018.08.021.
[69] Yadav S, Kumar P, Kumar A. Excess energy management and techno-economic analysis of optimal designed isolated microgrid with reliability and environmental aspects. Energ Conver Manage 2025;333:119772. https://doi.org/10.1016/j.enconman.2025.119772.
[70] Chen C, Wang F, Zhou B, Chan KW, Cao Y, Tan Y. An interval optimization based day-ahead scheduling scheme for renewable energy management in smart distribution systems. Energy Conver Manage 2015;106:584–96. https://doi.org/10.1016/j.enconman.2015.10.014.
[71] Hasani R, Mohammadi M, Samanfar A. Integrated multiobjective energy management for a smart microgrid incorporating electric vehicle charging stations and demand response programs under uncertainty. Int J Energy Res 2025;2025:9531493. https://doi.org/10.1155/er/9531493.
[72] Li L-L, Lou J-L, Tseng M-L, Lim MK, Tan RR. A hybrid dynamic economic environmental dispatch model for balancing operating costs and pollutant emissions in renewable energy: a novel improved mayfly algorithm. Expert Syst Appl 2022;203:117411. https://doi.org/10.1016/j.eswa.2022.117411.
[73] Li L, Wen T, Ji B, Xu H, Liu X. Two-tier optimization planning of electric integrated energy system with energy storage system for low-carbon parks. J Storage Mater 2025;123:116800. https://doi.org/10.1016/j.est.2025.116800.
[74] Abomazid AM, Farag HEZ. Optimal energy management of hydrogen energy facility using integrated battery energy storage and solar photovoltaic systems. EEE Trans Sustain Energy 2022;13:1457–68. https://doi.org/10.1109/TSTE.2022.3161891.
[75] Hernandez RR, Hoffacker MK, Field CB. Land-use efficiency of big solar. Environ Sci Technol 2014;48:1315–23. https://doi.org/10.1021/es4043726.
[76] Heeter J, Reames T. Incorporating energy justice into utility-scale photovoltaic deployment: a policy framework. Renew Energy Focus 2022;42:1–7. https://doi.org/10.1016/j.ref.2022.04.003.
[77] Khan FMNU, Rasul MG, Sayem ASM, Mandal N. Maximizing energy density of lithium-ion batteries for electric vehicles: a critical review. Energy Rep 2023;9:11–21. https://doi.org/10.1016/j.egyr.2023.08.069.
[78] NREL, 2024 Annual Rechnology Baseline - 2024 Electricity ATB Technologies, (2024). https://atb.nrel.gov/electricity/2024/technologies (accessed January 24, 2025).
[79] U. Cetinkaya, S. Demirbas, S. Ayik, R. Bayindir, Battery Energy Storage Systems in Different Countries for Arbitrage Services, in: 2023 11th International Conference on Smart Grid (icSmartGrid), 2023: pp. 1–5. DOI: 10.1109/icSmartGrid58556.2023.10170829.
[80] Wankouo Ngouleu CA, Koholé YW, Fohagui FCV, Tchuen G. Techno-economic analysis and optimal sizing of a battery-based and hydrogen-based standalone photovoltaic/wind hybrid system for rural electrification in Cameroon based on meta-heuristic techniques. Energy Conve Manage 2023;280:116794. https://doi.org/10.1016/j.enconman.2023.116794.
[81] Abdelqawee IM, Emam AW, ElBages MS, Ebrahim MA. Implementation of a novel hybrid optimizer for energy management of fuel cell/battery/supercapacitor system. Energy Syst 2022. https://doi.org/10.1007/s12667-022-00541-4.
[82] Y. Tanahashi, H. Kobayashi, Y. Nakamura, M. Aoki, Novel Optimization Method Hybridized by MILP and PSO for Operation Planning in Microgrid System, in: 2022 International Power Electronics Conference (IPEC-Himeji 2022- ECCE Asia), 2022: pp. 1359–1364. DOI: 10.23919/IPEC-Himeji2022-ECCE53331.2022.9807093.
[83] Sun Y, Cai Z, Zhang Z, Guo C, Ma G, Han Y. Coordinated energy scheduling of a distributed multi-microgrid system based on multi-agent decisions. Energies 2020;13:4077. https://doi.org/10.3390/en13164077.
[84] Li Q, Xiao X, Pu Y, Luo S, Liu H, Chen W. Hierarchical optimal scheduling method for regional integrated energy systems considering electricity-hydrogen shared energy. Appl Energy 2023;349:121670. https://doi.org/10.1016/j.apenergy.2023.121670.
[85] Tian T, Ma Z, Shu J, Bie K, Feng R, Ding J. Optimal sizing of hydrogen storage for a standalone microgrid. In: 2024 IEEE 2nd International Conference on Power Science and Technology (ICPST); 2024. p. 1342–7. https://doi.org/10.1109/ICPST61417.2024.10601858.
[86] Heleno M, Stadler M, Mashayekh S, Cardoso G, De Luís R. A novel deterministic and probabilistic dynamic security assessment approach for isolated microgrids. In: 2017 19th International Conference on Intelligent System Application to Power Systems (ISAP); 2017. p. 1–6. https://doi.org/10.1109/ISAP.2017.8071404.
[87] Sukumar S, Mokhlis H, Mekhilef S, Naidu K, Karimi M. Mix-mode energy management strategy and battery sizing for economic operation of grid-tied microgrid. Energy 2017;118:1322–33. https://doi.org/10.1016/j.energy.2016.11.018.
[88] Takada K, Ikegami T. Long-term planning model for a chp system using particle swarm optimization algorithm and mixed integer linear programming, in. Int Conf Smart Energy Syst Technol (SEST) 2018;2018:1–6. https://doi.org/10.1109/SEST.2018.8495672.